Atmospheric Environment 257 (2021) 118441

Contents lists available at ScienceDirect

Atmospheric Environment

journal homepage: www.elsevier.com/locate/atmosenv

Sensitivity analysis of the dust emission treatment in CMAQv5.2.1 and its application to long-range transport over East Asia

Steven Soon-Kai Kong [a], Joshua S. Fu [b], Xinyi Dong [b], Ming-Tung Chuang [c], Maggie Chel Gee Ooi [a,d], Wei-Syun Huang [a], Stephen M. Griffith [a], Shantanu Kumar Pani [a], Neng-Huei Lin [a,e,*]

[a] Department of Atmospheric Sciences, National Central University, Taoyuan, 32001, Taiwan
[b] Department of Civil and Environmental Engineering, The University of Tennessee, Knoxville, TN, 37996, USA
[c] Research Center for Environmental Changes, Academia Sinica, Taipei, 11529, Taiwan
[d] Institute of Climate Change, National University of Malaysia (UKM), Bangi, 43600, Malaysia
[e] Center for Environmental Monitoring and Technology, National Central University, Taoyuan, 32001, Taiwan

HIGHLIGHTS

- Most significant dust transport event in 6 years to northern Taiwan occurred in April 2018.
- Revised CMAQ dust emission treatment improved the modeled PM_{10} performance.
- Uplifted dust particles reached a maximum height of 500–700 hPa.
- Importance of improving the dust emission treatment over the marine boundary layer is highlighted.

GRAPHICAL ABSTRACT

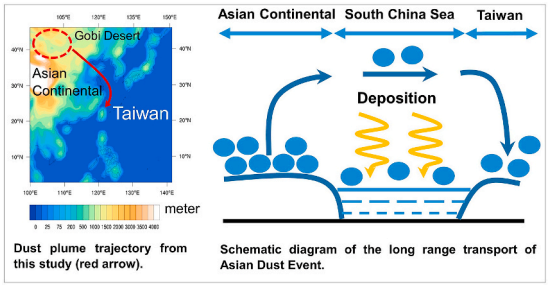

ARTICLE INFO

Keywords:
Air quality modeling
East asian dust event
Long-range transport
Taiwan

ABSTRACT

East Asian Dust (EAD) has had a measurable impact on global climate and air quality, including visibility and human health, in numerous locations around the globe over the past decade. The accuracy of an air quality modeling system to simulate dust events is vital for early warning systems. The most significant dust event observed in 6 years for northern Taiwan occurred during 4th–9th April 2018, and was characterized by high wind speeds (9–13 m s^{-1}) upon arrival to the region. We assessed the windblown dust emission treatment across various modifications and found better model performance by decreasing the soil moisture factor and updating the aerosol speciation profile over East Asia. In the optimized CMAQ simulation, uplifted dust particles reached a maximum height of 500–700 hPa, which is crucial for effective transport of the dust plume to the downwind Taiwan region. However, by tracking the vertical distribution profile, we found the model was insufficient to estimate dust aerosol after exiting from over the continent and entering the marine boundary layer. Our simulation indicated the dust event consisted of two plumes, where the first one was significantly impacted by wet deposition (−70.65%) from a rainfall belt stretching across Japan, Korea and the East China Sea. Then, low wind speed during a period of no precipitation over the marine area led to even greater dust deposition (−89.11%) from the second plume, resulting in a consistent negative bias for the simulation. This modeling study highlights

* Corresponding author. Department of Atmospheric Sciences, National Central University, Taoyuan, 32001, Taiwan.
E-mail address: nhlin@cc.ncu.edu.tw (N.-H. Lin).

https://doi.org/10.1016/j.atmosenv.2021.118441
Received 14 May 2020; Received in revised form 1 April 2021; Accepted 22 April 2021
Available online 5 May 2021

the importance of improving the dust emission treatment for a better simulation of dust aerosol transport over the marine boundary layer. To reduce the uncertainty in the dust outflow region, the deposition mechanisms for the CMAQ dust treatment should be revised.

1. Introduction

Mineral dust has been a public concern for some time as it degrades air quality (De Longueville et al., 2010), reduces visibility (Seinfeld et al., 2004), and alters the earth's radiation budget (Miller et al., 2006), hydrological processes (Zhao et al., 2011), and atmospheric chemistry (Dong et al., 2016; Wang et al., 2012). East Asian Dust (EAD) events, which largely originate in the Gobi and Taklamakan deserts (Han et al., 2010; Bian et al., 2011; Jing et al., 2017), have contributed to severe air pollution episodes especially in the East Asia region, including China (Zhao et al., 2011; Fu et al., 2013; Xu et al., 2017; Jiang et al., 2018; Tan et al., 2020), Korea (Park et al., 2012; Ghim et al., 2017), Japan (Eguchi et al., 2009; Uno et al., 2017), Hong Kong (Chow et al., 2014), and Taiwan (Tsai et al., 2013), but have also been shown to impact the remote Pacific Ocean (Wang et al., 2011, 2012), and the United States (Crooks et al., 2016). Moreover, dust particles influence the regional climate by cooling or warming the atmosphere (Huang et al., 2014, 2019; Chen et al., 2017; Dong et al., 2019). The mixing of dust and anthropogenic aerosol promote more warming in the atmosphere as compared to either anthropogenic aerosol or natural dust (Huang et al., 2014; Tian et al., 2018; Hu et al., 2019). On the other hand, meteorological conditions such as precipitation and wind speed can lead to variations in the dust aerosol concentration (Guo et al., 2019).

CMAQ is a state-of-the-science air quality model developed by the United States Environmental Protection Agency (US EPA), which has shown good predictive capability for dust aerosol concentrations over the continental United States (CONUS) (Appel et al., 2013). Implementation of a physical dust scheme in CMAQ for simulations over East Asia has been widely discussed as an alternative to simply changing the dust emission factor to that used for North America (Wang et al., 2012; Fu et al., 2014; Dong et al., 2016). Dong et al. (2016) introduced a dust module that double counted the soil moisture impact and updated the source dependent speciation profile for dust emission in CMAQv5.0 over East Asia. In CMAQv5.2.1, Foroutan et al. (2017) incorporated a new windblown dust emission treatment developed from a recent surface roughness length formulation, which itself was derived from field and laboratory study results of small-scale Aeolian processes. Foroutan et al. (2017) showed that simulated PM_{10} concentrations over the southwest United States in spring 2011 compared well with measurements. The NMB of PM_{10} improved from −60.1% (CMAQ without dust treatment) to −19.2% (CMAQ with new dust emission treatment). However, there have not been any attempts to incorporate the modifications demonstrated by Dong et al. (2016) for EAD scenarios into the updated CMAQ dust treatment presented by Foroutan et al. (2017). Furthermore, CMAQ simulation of dust aerosol transport through the marine boundary layer to receptor sites outside the Asian continent has also not been explored. Taiwan is a maritime island located southeast of China, and is highly affected by the long-range transport (LRT) of EAD aerosols during the winter and spring seasons when northeasterly winds prevail (Wang et al., 2011, 2012; Tsai et al., 2013); thus is an ideal receptor site for further evaluation of the CMAQ dust scheme. Dust transport in East Asia is largely determined by meteorological conditions, with the corresponding favorable characteristics described by Tsai et al. (2008), although some synoptic features favoring dust aerosol transport from the source region to Taiwan are still unclear.

A major dust outbreak occurred over East Asia on 4th–9th April 2018. This dust storm originated from the desert regions of northern China and Mongolia (Taklimakan and Gobi Deserts) and transported to downwind regions of the western north Pacific as depicted from satellite images (See Section 2.4). Therefore, in this study, a high spatial resolution

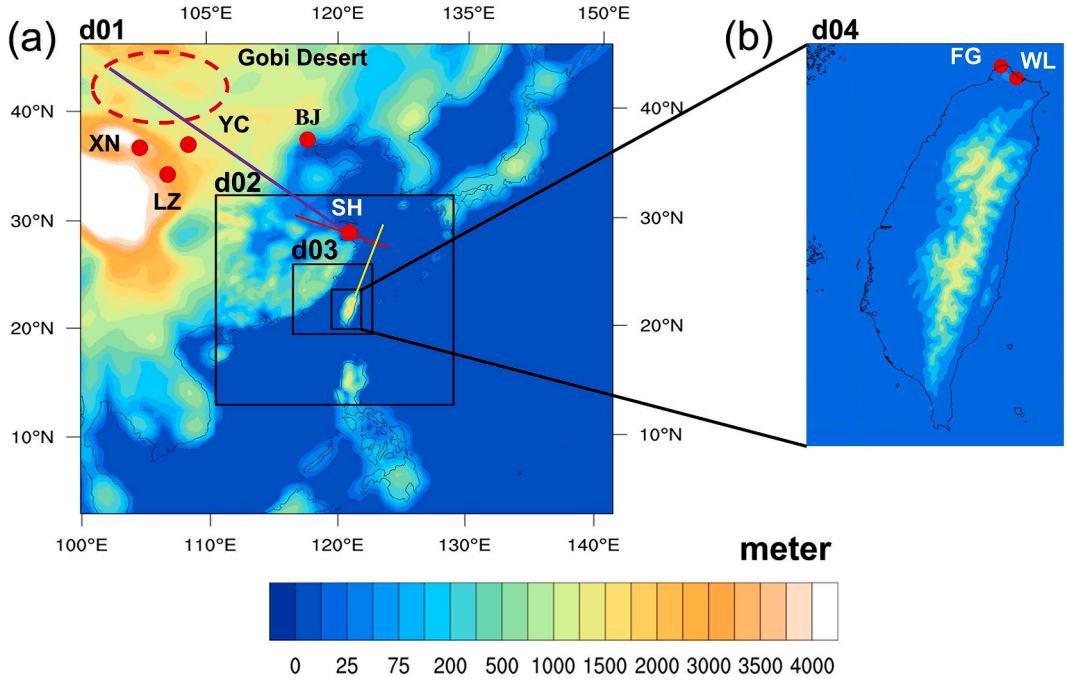

Fig. 1. (a) Modeling domain configuration where the purple, red, and yellow lines represent the transects that the dust aerosol plumes traveled along in this study and that are discussed in Section 5; air quality measurement stations (red markers) in Lanzhou (LZ), Xining (XN), Yinchuan (YC), Beijing (BJ), Shanghai (SH), and (b) northern Taiwan: Wanli (WL) and Cape Fuguei (FG) are used in this study. (For interpretation of the references to color in this figure legend, the reader is referred to the Web version of this article.)

Table 1
The details about simulation scenarios.

Scenarios	Descriptions
DUST_Off	Without in-line calculation of dust.
DUST_Default	With the new default wind-blown dust treatment (Foroutan et al., 2017).
DUST_Modified_1	Modified the soil moisture factor, f_m, to 0.1 (Darmenova et al., 2009).
DUST_Modified_2	Modified the dust emission speciation profile for the Gobi Desert (Huang et al., 2010; Dong et al., 2016).
DUST_Modified_3	Same as DUST_Modified_1, but with implementation of the new dust emission speciation profile.

Table 2
Default and new dust emission speciation profiles for the Gobi Desert.

Species	Model species	Mass contributions (%)			
		Default		New[a]	
		Fine mode	Coarse mode	Fine mode	Coarse mode
Sulfate	ASO4	2.50	0.95	2.66	0.47
Nitrate	ANO3	0.02	0.20	0.16	0.084
Chlorite	ACL	0.95	0.54	1.19	0.094
Ammonium	ANH4	0.005	0.35	0.00	0.19
Sodium	ANA	3.94	1.02	0.00	0.30
Calcium	ACA	7.94	1.79	0.00	1.08
Magnesium	AMG	0.00	0.80	0.00	0.82
Potassium	AK	3.77	0.28	0.00	0.12
Primary organic carbon	APOC	1.08	1.08	0.00	0.00
Non-carbon organic matter	APNCOM	0.43	0.43	0.00	0.00
Elementary carbon	AEC	0.00	0.00	0.00	0.00
Iron	AFE	3.36	2.43	0.00	3.06
Aluminum	AAL	5.70	4.27	0.00	4.64
Silicon	ASI	19.43	14.93	0.00	16.25
Titanium	ATI	0.28	0.34	0.00	0.37
Manganese	AMN	0.12	0.063	0.00	0.070
Water	AH2O	0.54	0.54	0.00	0.00
Unspeciated	AOTHR	50.22	70.00	0.00	0.00
Non-anion dust	ASOIL	0.00	0.00	95.99	72.46

[a] Dong et al. (2016).

CMAQv5.2.1 simulation with inline dust treatment was conducted to understand the source, transport and the impact of East Asian dust particles on air quality in Taiwan. CMAQ modeling with the new windblown dust treatment was applied for the East Asia and Taiwan domains. Moreover, we demonstrated an effective way to evaluate the dust module over East Asia and addressed the following questions:

1. How does the dust treatment developed by Foroutan et al. (2017) perform in modeling PM_{10} over East Asia? What are the most effective methods in the dust treatment for improving the simulations over East Asia?
2. What are the synoptic weather patterns associated with the LRT of EAD over East Asia?
3. Is CMAQ with the physical dust scheme able to capture dust aerosol transport beyond the Asian continent? What physical processes impact dust particles during passage through the marine boundary layer?

2. Methodology

2.1. Physical parameterization of windblown dust emission

Saltation or sandblasting is the main physical mechanism for dust emission. The onset of saltation caused by the wind, horizontal movement of sand (Kok et al., 2012) particles, and the vertical flux of dust are the first, second, and final stages, respectively (Foroutan et al., 2017). Dust particles can be lifted when the horizontal wind speed exceeds the threshold friction velocity, which is the minimum surface shear stress for saltation to occur (Shao et al., 2011). The threshold friction velocity ($u_{*,t}$) is calculated by the model as below:

$$u_{*,t} = u_{*,\,to}\, f_m\, f_r \tag{1}$$

where f_m and f_r are the correction factors of soil moisture and surface roughness, respectively, and $u_{*,to}$ is the ideal threshold friction velocity.

Foroutan et al. (2017) developed the new dust emission treatment by integrating the windspeed, soil texture, soil moisture, and surface roughness length derived from field and laboratory study. The surface roughness length (z_o) was modulated with a critical value (λ) of 0.2 (Shao and Yang, 2005) as shown below:

$$z_o \Big/ h = \begin{cases} 0.96\,\lambda^{1.07}, \lambda < 0.2 \\ 0.083\,\lambda^{-0.46}, \lambda \geq 0.2 \end{cases} \tag{2}$$

where h is the effective height of roughness elements. According to Shao and Yang (2005), z_o increases with the increase of λ to a maximum value of 0.2, and then decreases as λ further increases.

2.2. Numerical model and experiments

Simulations over the East Asia region were carried out with a coarse domain of 81 km, and nested towards the Taiwan region at resolutions of 27 km, 9 km, and 3 km (Fig. 1a). The coarse domain covers the East Asia region including the Gobi Desert, which is the main dust source region in East Asia during the spring season. (Bian et al., 2011). The meteorological simulation utilizing the Weather Research Forecast (WRF) model version 3.9.1 was based on a two-way nesting technique in which NCEP Global Forecast System (GFS) output was used as the initial condition. The meteorological fields together with the emission inventory were used to drive the air quality model. The present study utilized CMAQ model version 5.2.1, with chemistry represented by the Carbon Bond V (CB05) gas-phase chemical mechanism in the aerosol module (AERO6).

The anthropogenic emission data for East Asia, including domains 1, 2 and 3, were obtained from the MICS-Asia (Model Inter-comparison Study for Asia) Phase III emission inventory (Li et al., 2017). Our work modified the emissions of SO_2 (−62%), NO_x (−17%), NMVOC (+11%), NH_3 (+1%), CO (−27%), PM_{10} (−38%), $PM_{2.5}$ (−35%), BC (−27%), OC (−35%) and CO_2 (+18%) by referring to the relative changes of China's anthropogenic emissions between 2010 and 2017 (Zheng et al., 2018). Meanwhile, TEDS 9.0 (Taiwan Emission Database System, TWEPA, 2011; https://erdb.epa.gov.tw/) was used for domain 4. The biogenic emissions were prepared by the Biogenic Emission Inventory System version 3.09 (BEIS3, Vukovich and Pierce, 2002) for Taiwan and Model of Emissions of Gases and Aerosols from Nature v2.1 (MEGAN, Guenther et al., 2012) for regions outside Taiwan. CMAQ numerical simulations of particulate matter were based on the sum of the accumulation and Aitken modes of sulfate mass (ASO_4), ammonium mass (ANH_4), nitrate mass (ANO_3), organic matter mass (AOM), organic carbon mass (AOC), elemental carbon mass (AEC), unspecified anthropogenic mass (AOTHR) and coarse mode marine/soil-derive/unspecified anthropogenic mass (ASEACAT/ASOIL/ACORS) (Appel et al., 2013).

Emission inventories are a driver of 3D air quality models like CMAQ and anthropogenic emissions are a major component underlying aerosol formation, accumulation and transformation. To capture only dust emissions would omit an important fraction of fine and coarse aerosol mode development; thus the anthropogenic emission inventory is described here in limited detail. To study the performance of CMAQ with the dust treatment, we carried out a series of sensitivity simulations by using the indices defined in Chang and Hanna (2004) and TWEPA (2016), such as Normalized Mean Bias (NMB), Factor of Two (FAC2), Correlation coefficient (R) and Index of Agreement (IOA). Simulation

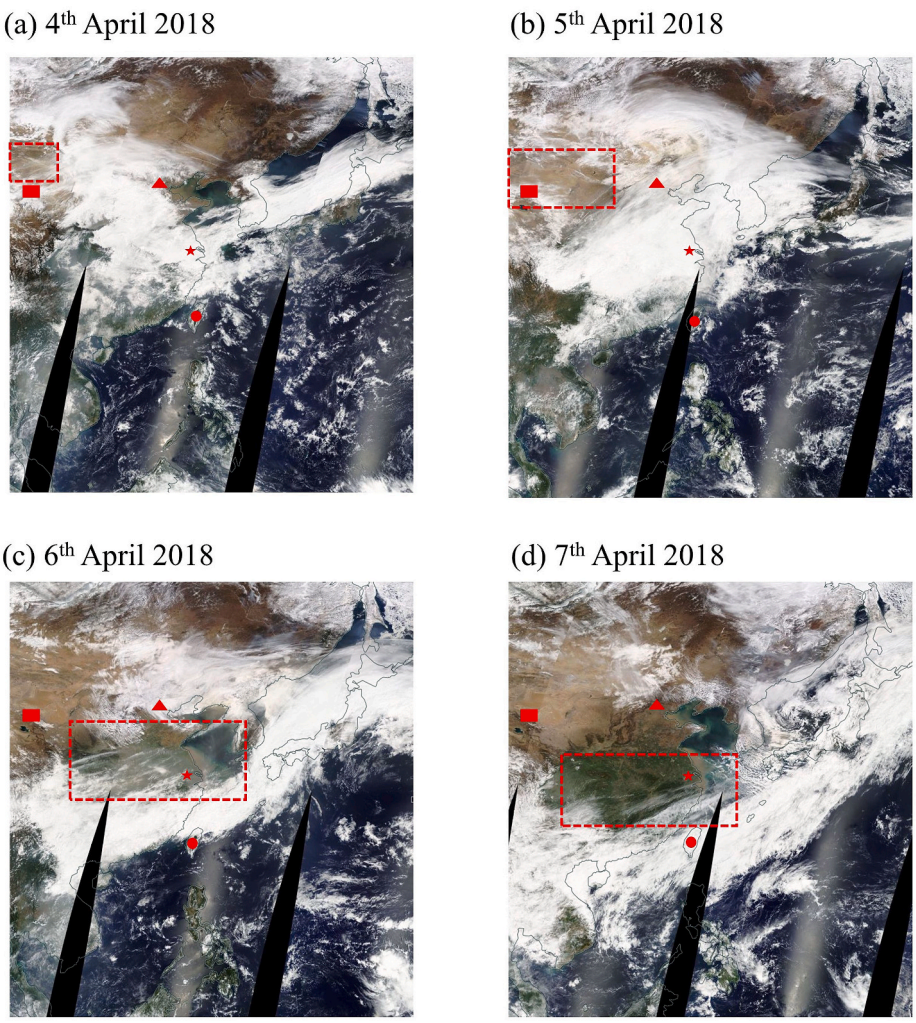

Fig. 2. MODIS Terra images showing dust outbreak across East Asia from 4th–7th April 2018. Red Rectangular, triangle, star and circle indicate Lanzhou, Beijing, Shanghai and Taiwan. The red rectangular box with dash line indicates the dust lifting, transport and distribution. (For interpretation of the references to color in this figure legend, the reader is referred to the Web version of this article.)

results were compared by various statistical methods with measured data from China Air Quality Online Analysis Platform (https://www.aqistudy.cn/) and Taiwan Environmental Protection Administration (TWEPA).

Table 1 presents the five simulation scenarios, namely DUST_Off, DUST_Default, DUST_Modified_1, DUST_Modified_2 and DUST_Modified_3, and the responding descriptions. DUST_Off did not consider in-line calculation of the dust treatment, while DUST_Default included the wind-blown dust emission treatment modulated by Foroutan et al. (2017). The size of the dust particle in CMAQ is divided into four size bins (0.1–1.0 μm; 1.0–2.5 μm; 2.5–5.0 μm; 5.0–10.0 μm). The first two bins are the fine-aerosol mode and the second two bins are the coarse-aerosol mode, with geometric mean diameters of 1.3914 μm and 5.2590 μm, respectively. Moreover, the generated dust mass was split into 7% and 93% for the fine and coarse mode, respectively. DUST_Modified_1 revised f_m from 1.0 to 0.1 to reduce the soil moisture impact, because the NOAH land surface model used by CMAQ references soil moisture values by 10 cm depth, which is not appropriate for dust aerosol suspensions occurring at the surface (Darmenova et al., 2009; Foroutan et al., 2017).

The dust treatment has been examined over the continental United States; however, simulations of dust events in East Asia have not been thoroughly addressed. Based on local measurements (Huang et al., 2010), Dong et al. (2016) developed a source-dependent species profile for the Gobi desert to better depict the dust aerosol in CMAQ. The new species profile by Dong et al. (2016), which is itself based on ratios of aerosol components measured by Huang et al. (2010), is compared to the default set up in the model and is shown in Table 2. The new model species consist of anions: sulfate (ASO_4), nitrate (ANO_3), chloride (ACL); cations: ammonium (ANH_4), sodium (ANA), calcium (ACA), magnesium (AMG) and potassium (AK); and elements: iron (AFE), aluminum (AAL), silicon (ASI), titanium (ATI) and manganese (AMN). Certain species that were not measured by Huang et al. (2010) are kept the same as the default profile, such as primary organic carbons (APOC), non-carbon aerosols (APNCOM), elementary carbons (AEC), silicon (ASI) and water (AH_2O). The contributions of other species are defined as unspecified (AOTHR) and non-anion dust (ASOIL). As a result, the simulation of DUST_ Modified_2 included the new dust emission speciation profile for the Gobi Desert (Table 2). Eventually, we re-ran the model by considering the combination of the two modified treatments. Thus, DUST_Modified_3 combined the DUST_Modified_1 and DUST_Modified_2 treatment, by revising f_m from 1.0 to 0.1 to reduce the soil moisture impact (Darmenova et al., 2009), and at the same time utilized the source-dependent species profile for the Gobi desert in an attempt to optimize the dust model performance.

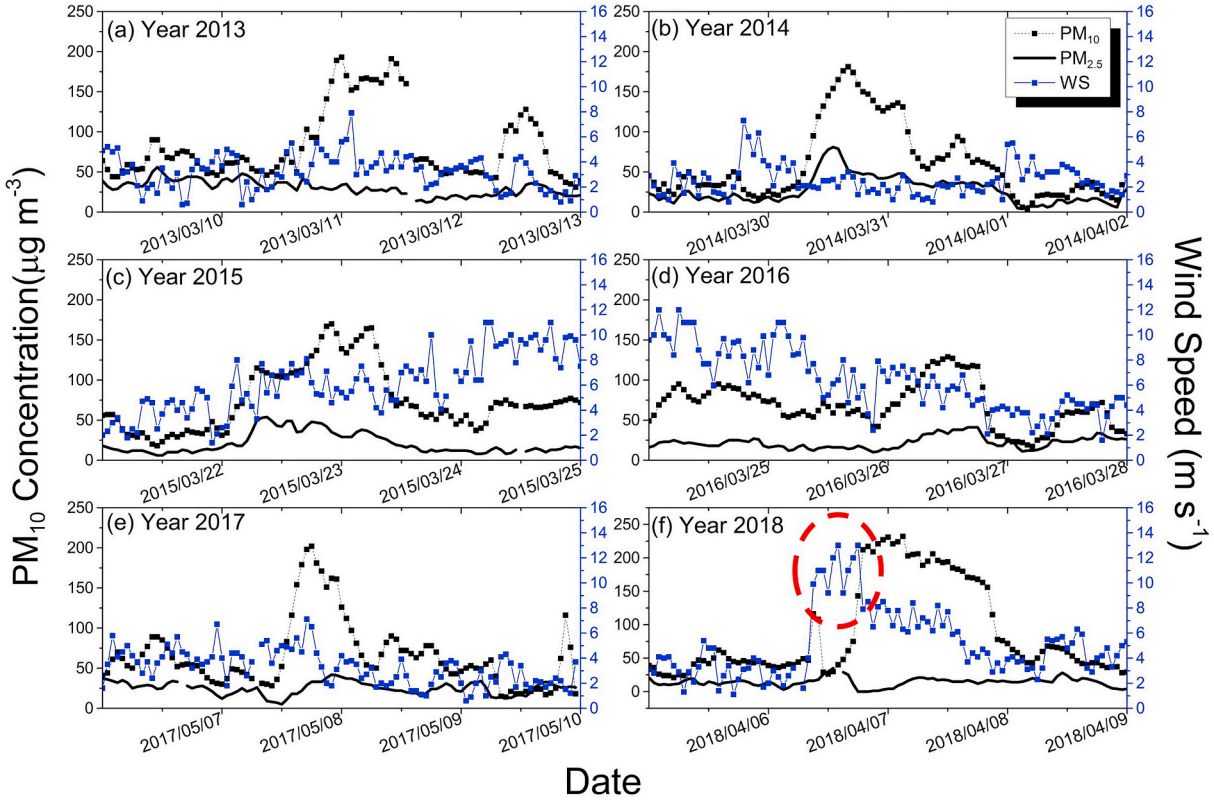

Fig. 3. Time series of hourly average surface PM_{10} and $PM_{2.5}$ concentrations and wind speed at Wanli station during six dust events in year (a) 2013, (b) 2014, (c) 2015, (d) 2016, (e) 2017 and (f) 2018.

Table 3
Measured versus modeled evaluation of meteorological conditions in East Asia during 4th–9th April 2018.

		Stations		
		Yinchuan	Cape Fuguei	Wanli
Temperature	NMB (%)	−2.72	−0.88	−1.71
	FAC2	0.97	0.99	0.98
	R	0.90	0.96	0.97
	IOA	1.00	1.00	1.00
Wind Speed	NMB (%)	−42.62	7.76	−15.38
	FAC2	0.57	1.08	0.85
	R	0.81	0.90	0.73
	IOA	0.92	1.00	0.99

Note: the definition of the statistical formulas NMB: Normalized Mean Bias; FAC2: Factor of Two; R: Correlation Coefficient and IOA: Index of Agreement.

Table 4
Evaluation of PM_{10} concentrations in East Asia.

	Simulation Scenarios				
	Off	Default	Modified_1	Modified_2	Modified_3
NMB (%)	−83.76	−78.51	−52.36	−50.64	−23.14
FAC2	0.24	0.29	0.50	0.51	0.76
R	−0.13	0.21	0.39	0.40	0.41
IOA	0.38	0.52	0.76	0.77	0.89

Note: the definition of the statistical formulas NMB: Normalized Mean Bias; FAC2: Factor of Two; R: Correlation Coefficient and IOA: Index of Agreement.

2.3. Ancillary datasets

PM_{10} (particulate matter ≤10 μm in aerodynamic diameter) and $PM_{2.5}$ (particulate matter ≤2.5 μm in aerodynamic diameter) concentrations during six dust events in 2013–2018 were obtained from the Wanli air quality monitoring station in northern Taiwan maintained by the Taiwan Environmental Protection Agency (EPA). In addition, both PM_{10} and $PM_{2.5}$ concentrations within the mainland China in April 2018 were obtained from China Air Quality Online Monitoring and Analysis Platform (https://www.aqistudy.cn). Moderate Resolution Imaging Spectroradiometer (MODIS) Terra satellite images were obtained from the U.S. National Aeronautics and Space Administration (https://worldview.earthdata.nasa.gov/) to visualize dust outbreaks across East Asia. In order to obtain the vertical distributions of aerosol subtype information for the dust plume, the Cloud-Aerosol Lidar and Infrared Pathfinder Satellite Observations (CALIPSO) data archive was accessed for the study period (3rd and 4th April 2018; nighttime data) via https://www-calipso.larc.nasa.gov/products/lidar/. In order to demonstrate the spatiotemporal distribution of dust without the influence of clouds, the Modern Era Retrospective-analysis for Research and Application version 2 (MERRA-2) reanalysis data was used in this study. MERRA-2 (Gelaro et al., 2017) is a NASA reanalysis utilizing Goddard Earth Observing System Data Assimilation System Version 5 (GEOS-5) and covering remotely sensed data at a native spatial resolution of 0.5 ° × 0.625 °. Ultraviolet Aerosol Index (UVAI) is ideal parameter for tracking the evolution of episodic aerosol plumes from dust outbreaks, volcanic ash, and biomass-burning. The UVAI data (product name: OMTO3d V3) was obtained from the Ozone Monitoring Instrument (OMI). In this study, UVAI is used to visualize the dust transport in East Asia.

2.4. The East Asian Dust episode

Fig. 2 shows the severe dust outbreak that developed over East Asia and transported towards the western North Pacific during 4th–9th April 2018 as visualized from the MODIS Terra sensor. Although cloud cover partially obscured the dust distribution and transport, MODIS Terra

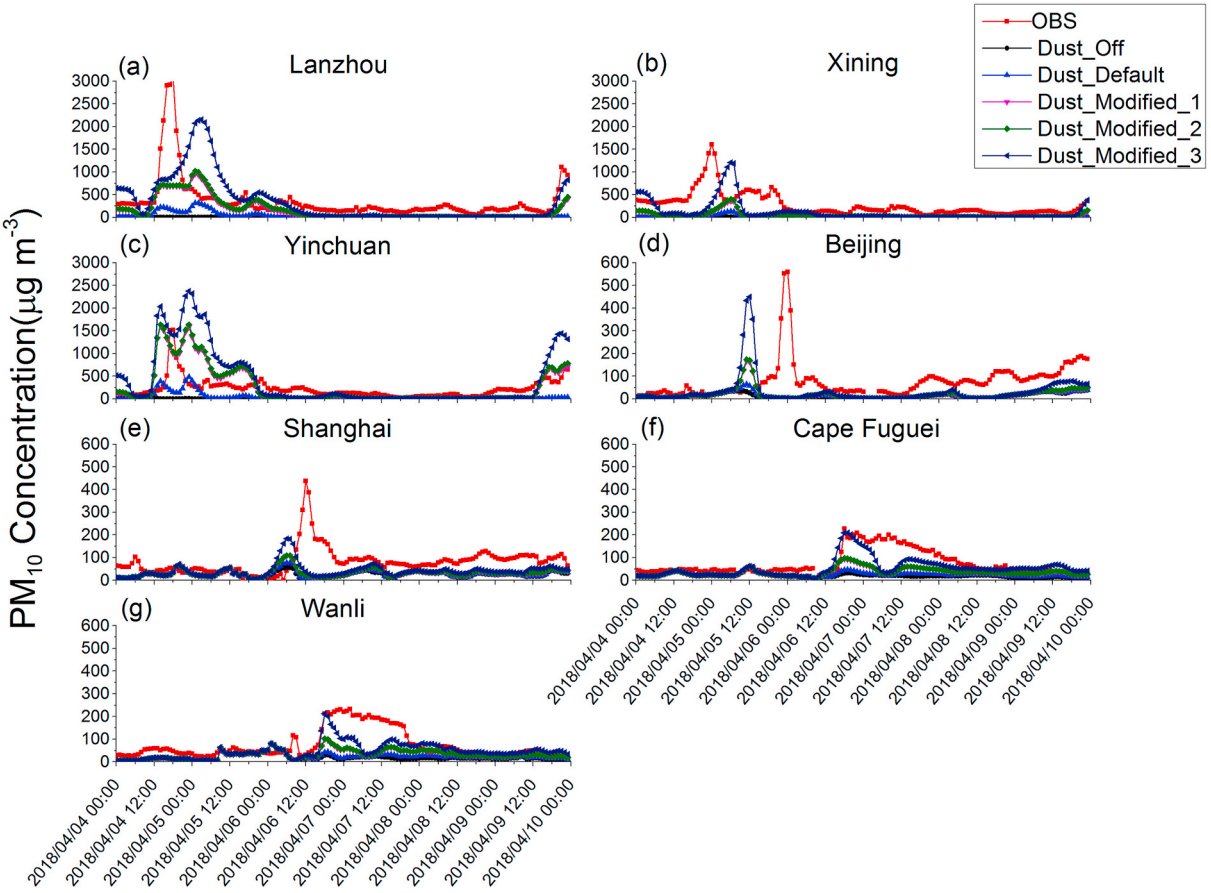

Fig. 4. Time series of modeled and measured dust aerosol over (a) Lanzhou, (b) Xining, (c) Yinchuan, (d) Beijing, (e) Shanghai, (f) Cape Fuguei and (g) Wanli.

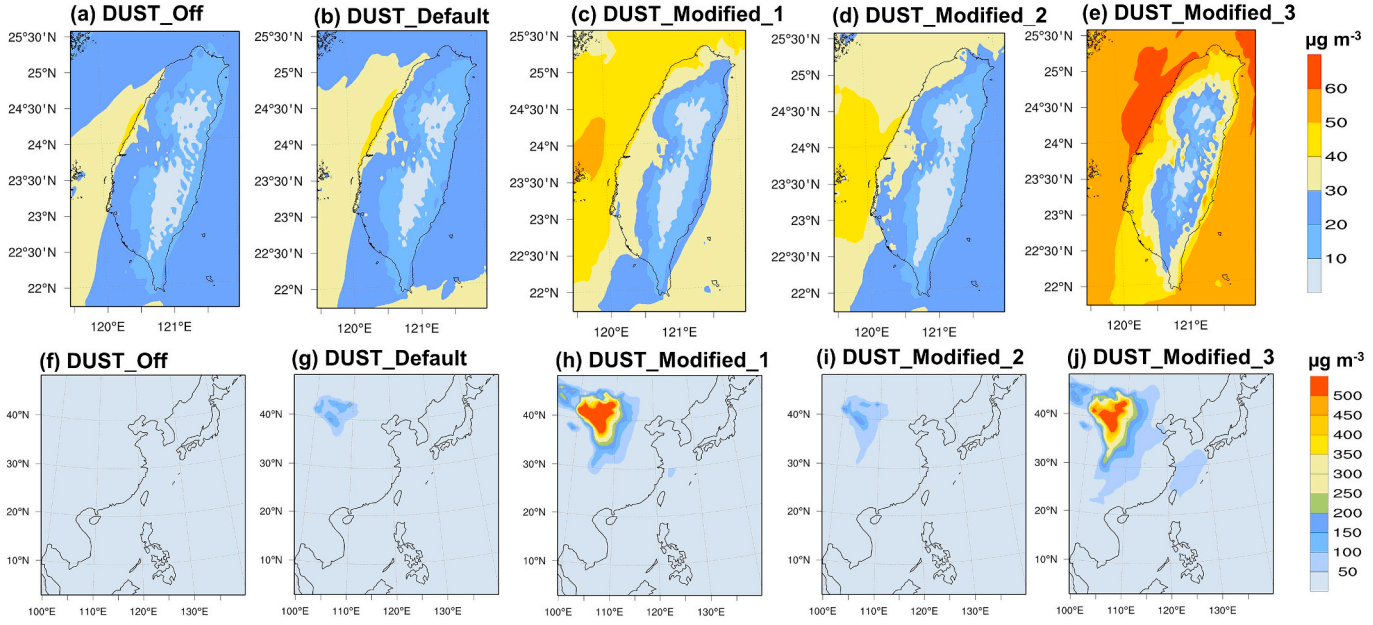

Fig. 5. Daily average modeled PM_{10} concentration over Taiwan (a–e) and East Asia (f–j) under the following schemes: (a, f) Dust_Off, (b, g) Dust_Default, (c, h) Dust_Modified_1, (d, i) Dust_Modified_2 and (e, j) Dust_Modified_3.

verifies that the dust was present in northwest China on 4th–5th April and then present over Shanghai and Taiwan on 6th and 7th April, respectively. The observed PM_{10} and $PM_{2.5}$ concentrations at Wanli air quality monitoring station in northern Taiwan during six dust events in 2013–2018 are presented in Fig. 3. During the most recent event, 6th–7th April 2018, PM_{10} increased by ~143 μg m^{-3} in just 2 h, and eventually peaked at 231 μg m^{-3} on 00 LST 7th April, while $PM_{2.5}$ was only 4 μg m^{-3}. The dust event was characterized by initially high wind speeds

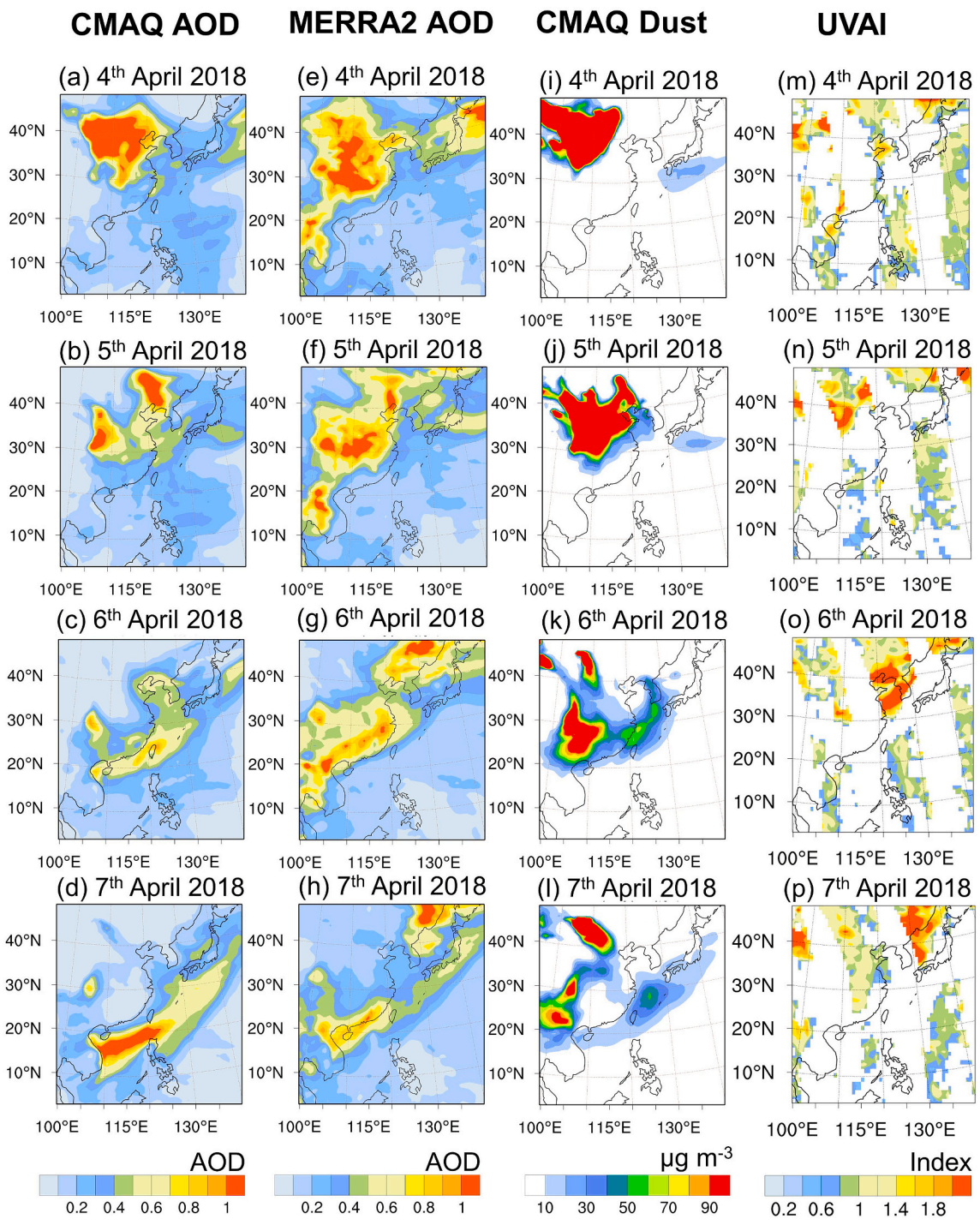

Fig. 6. Comparison of (a–d) CMAQ AOD spatial distribution over East Asia to that from (e–h) MERRA reanalysis; (i–l) mineral dust of CMAQ results and the (m–p) ultraviolet aerosol index (UVAI) over East Asia obtained from OMI.

(9–13 m s^{-1}) at Wanli station (red circle in Fig. 1), with PM_{10} concentrations >126 μg m^{-3} persisting for a total of 27 h on 6th–7th April 2018, making it the longest dust event observed in 6 years for northern Taiwan. The high PM_{10} episode could be largely associated with the significant dust storm that swept over East Asia. The vertical distribution of aerosol subtypes, as depicted from CALIPSO (Supplement Fig. S1) also shows the large emission of dust over northern China and its downwind region during the above-mentioned period. Dust reached to 10 km above ground level, indicating the severity of the outbreak.

3. Model evaluation

3.1. Evaluation of WRF model

The dust aerosol concentration simulated by CMAQ is dependent on meteorological conditions such as surface temperature and wind speed. This section evaluates the performance of the WRF model in simulating the surface meteorology over domain 1, using Yinchuan as the representative site, and domain 4, using the Cape Fuguei and Wanli sites, by comparing with the observed data from the weather database WMO SYNOPS (http://www.meteomanz.com/?l=1) and TWEPA,

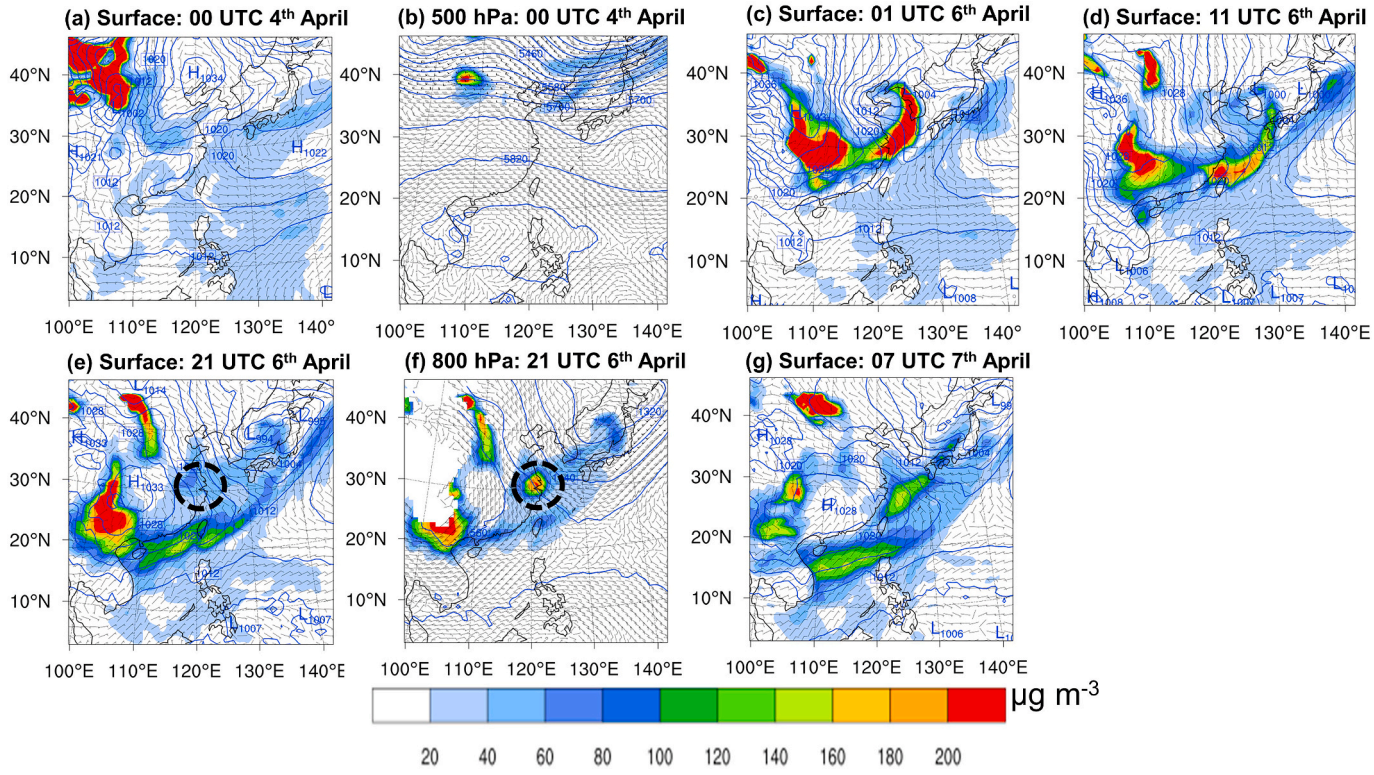

Fig. 7. Spatial distribution of the wind field and PM_{10} concentrations (colored) at (a) 00 UTC 4th (surface), (b) 00 UTC 4th (500-hPa), (c) 01 UTC 6th (surface), (d) 11 UTC 6th (surface), (e) 21 UTC 6th (surface), (f) 21 UTC 6th (800-hPa), and (g) 07 UTC 7th (surface) April 2018.

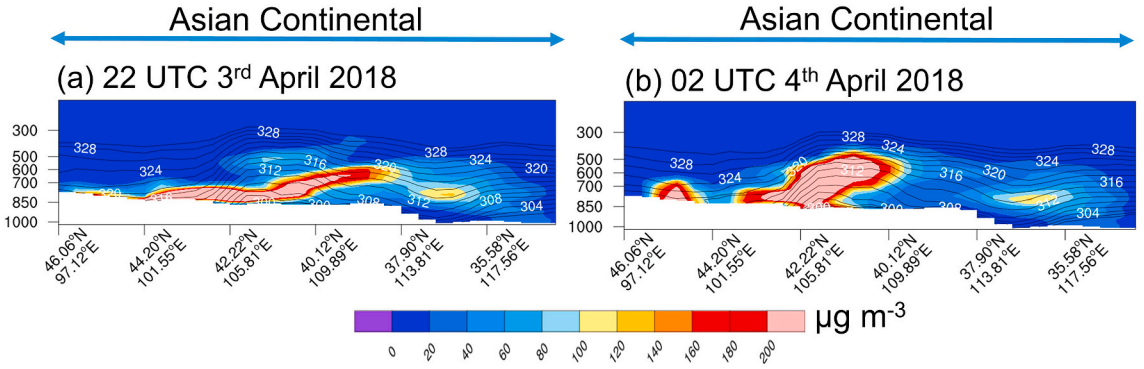

Fig. 8. Spatial distribution of potential temperature (dark contour from 300 to 330 K by 2 K) and vertical cross section of PM_{10} concentrations at (a) 22 UTC 3rd and (b) 02 UTC 4th April 2018. The x-axis is the transect represented by the purple line in Fig. 1(a). (For interpretation of the references to color in this figure legend, the reader is referred to the Web version of this article.)

respectively. Evaluation of the WRF simulation was conducted by using a statistical index (Emery et al., 2001; Chang and Hanna, 2004): Normalized Mean Bias (NMB), Factor of Two (FAC2), Correlation coefficient (R) and Index of Agreement (IOA) (Table 3). In general, WRF performed well in modeling surface temperatures and wind speed yielding significant Relation ($R > 0.3$) at all stations. In addition, the model showed almost perfect performance in surface temperature simulation ($IOA = 1.0$). The modeled wind speed performance over Cape Fuguei and Wanli were better than at Yinchuan, which could be due to the poor representation of steep terrains with a coarse grid resolution over domain 1 (Wang et al., 2012).

3.2. Impact of new dust treatment on CMAQ modeling

CMAQ modeling performance for PM_{10} was evaluated by the statistical index parameters noted above, such as NMB, FAC2, R and IOA (Table 4). The measured and modeled values from the source region including Lanzhou, Xining, Yinchuan, Beijing and Shanghai, and the reception such as Cape Fuguei and Wanli were compared. In general, the results from DUST_Off and DUST_Default were not distinctly different, both having underestimated the measured values, leading to NMB of −83.76% and −78.51%, respectively. Our results were consistent with Fu et al. (2014) and Dong et al. (2016), where both studies indicated a large model underestimation of PM_{10} concentrations over East Asia by −72.2% and −55.4%, respectively. Hence, revising the dust scheme to represent the different geographical influences in East Asia and the US is vital. DUST_Modified_1 simulations increased the modeled PM_{10} concentrations, resulting in a NMB of −52.36%, which was much better than DUST_Off and DUST_Default. In other words, the process of reducing the soil moisture as suggested by Darmenova et al. (2009) could effectively free more dust particles from the ground in the source region and transport them to receptor locations (e.g. northern Taiwan).

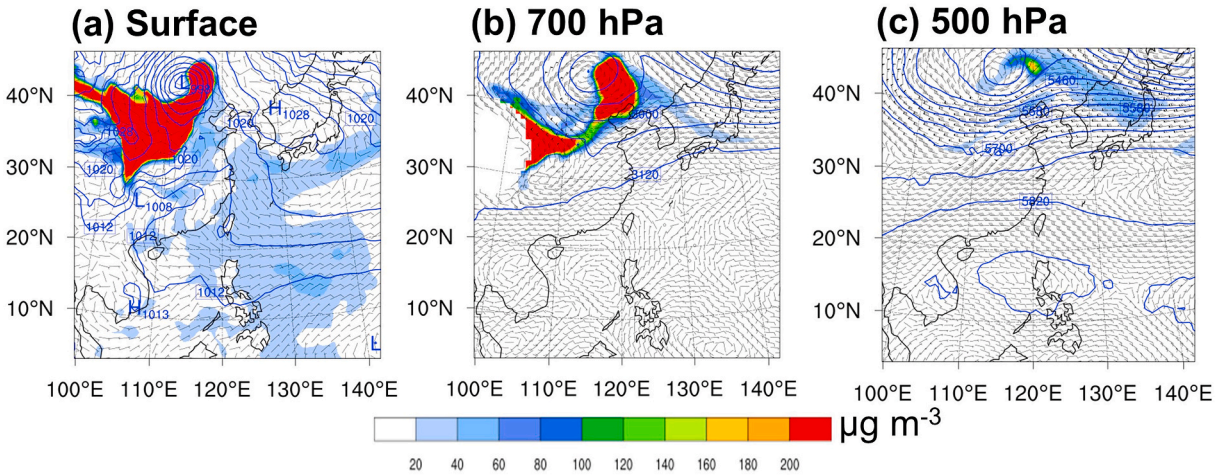

Fig. 9. The spatial distribution of the wind field and PM_{10} concentration (colored) at the (a) surface, (b) 700 hPa and (c) 500 hPa on 5th April 2018.

Dong et al. (2016) suggested that the default species profile within the dust treatment might not reasonably represent East Asia dust source conditions. Hence, a new speciation profile of dust emission from the Gobi Desert was implemented as shown in Table 2. Compared to Dust_Modified_1, Dust_Modified_2 resulted in a better NMB of −50.64%, although it was still a slight improvement over the default dust treatment. Combining the modified dust treatments is important for optimizing the performance across all limitations and tailoring it for use in the study location. Dust_Modified_3 resulted in further NMB improvement to −23.14%, by combining both the modified soil moisture factor and modified dust source profile. Generally, the time series of DUST_Modified_3 is the most satisfying relative to individual modified dust treatments when comparing measured and modeled results (Fig. 4). For instance, the time series of both measured and modeled PM_{10} concentration over the source region such as Lanzhou station showed a similar trend particularly in capturing the peak value, with a time lag of 10 h between the both peaks. Meanwhile, PM_{10} at the downwind region Cape Fuguei peaked at 222.8 μg m^{-3} in the DUST_Modified_3 simulation, which is only 5.8 μg m^{-3} less than the observed peaked value, and is much higher than the peak PM_{10} concentrations of 120.1 μg m^{-3} and 81.1 μg m^{-3} from DUST_Modified_1 and DUST_Modified_2, respectively.

The spatial distributions of daily average PM_{10} from the various simulations are shown in Fig. 5. For the Dust_Off scenario, average PM_{10} was less than 30.0 μg m^{-3} over the whole Taiwan modeling domain (as shown in Fig. 5a). A similar spatial distribution pattern was found from the Dust_Default simulation, indicating no significant dust particle concentrations were captured by the model in this region. Hence, this leads to a similar concern as before that the original CMAQ dust treatment is not appropriate for use in East Asia (Fig. 5b). The insignificant PM_{10} concentrations simulated over Taiwan by DUST_default were attributed directly to ineffective lifting of the dust particles in the source region of northern China (Fig. 5f and g). Meanwhile, the simulations of each individual modified dust scheme (i.e. Dust_Modified_1, and _2) successfully emitted and transported a portion of the dust particles from the source region, but resulted in PM_{10} of only 30.0–40.0 μg m^{-3} over northern and western Taiwan (Fig. 5c and d). As shown in Fig. 5e, high PM_{10} concentrations were simulated by the combined scheme DUST_Modified_3, averaging more than 40.0 μg m^{-3} over the ocean, and over northern and western Taiwan. Furthermore, average PM_{10} over the source region was less than 500.0 μg m^{-3} by Dust_Modified_3 (Fig. 5j). From the simulations of the dust episode, transported dust aerosol contributed 79.3% of the surface PM_{10} concentrations over northern Taiwan, which is consistent with measurements in Shanghai by 76.8% (Huang et al., 2012) and modeling work simulated in the Yangtze River Delta by 78.9% (Fu et al., 2014) during dust events in 2009 and 2011, respectively.

Modeled surface PM_{10} concentrations were reasonably well simulated with the ground measurements. Nevertheless, it is vital to verify the total dust emission from the source region. As the mean dust emission flux was simulated by CMAQ model, a high emission flux over northwest China was observed from the model indicating the East Asian dust source region (Supplement Fig. S2). The mean dust emission flux from 4th–7th April 2018 was more than 60 μg m^{-2} s^{-1}, which is similar to that simulated by Tan et al. (2017) in 2010 in western China and Gobi desert.

Fig. 6 shows the spatial distribution of daily averaged AOD derived from CMAQ and MERRA2 reanalysis during the dust event. It was observed that the measured and simulated AOD generally agreed well with each other during 4th–5th April 2018 when the massive dust storm occurred over the Asian continent (Fig. 6a, b, 6e and 6f). The high AOD value above 0.5 indicated that the pollution may have a high contribution from dust particles (Han et al., 2012). The dust was gradually transported toward the downwind areas on 6th–7th April 2018 (Fig. 6c, d, 6g and 6h)). In this period, high AOD values were found in southern China and continental Southeast Asia as suggested by MERRA2 reanalysis, which may have additional contribution from biomass burning in this particular region. Hence, it is suggested that the model is able to reproduce the AOD MERRA2, at the same time showing the source of the dust event originating in northwest China.

The main component of PM_{10} especially mineral dust is vital for analysis and evaluation of the LRT and can be monitored by the UV aerosol index (UVAI) from Ozone Monitoring Instrument observations. UV aerosol index is calculated by estimating the difference of two UV wavelengths. Positive value of UVAI indicates UV is absorbed by a large amount of aerosols such as volcanic ash, black carbon and mineral dust from the desert. Fig. 6i–p shows the spatial distribution of satellite UVAI over East Asia during 6th–7th April 2018. The model results agree well with the CMAQ simulations where both datasets illustrate a massive dust event over the Gobi Desert on 4th April 2018 (Fig. 6i and m). On 5th April 2018, the dust plume gradually transported toward northern China as shown in Fig. 6j and n. Finally, a high portion of mineral dust was found reaching downwind areas such as the Korea Peninsula and Taiwan (Fig. 6k and o).

4. Characteristics of the dust event during transport to Taiwan

While focusing on the DUST_Modified_3 simulation, we attempted to characterize the controlling mechanism of long-range dust transport from northern China to northern Taiwan. The weather pattern during the April 2018 dust event was characterized as High Pressure Peripheral Circulation (HPPC), following Chuang et al. (2008a). The high-pressure center was located at 30°N, near the Asian continent (Fig. 7a). The

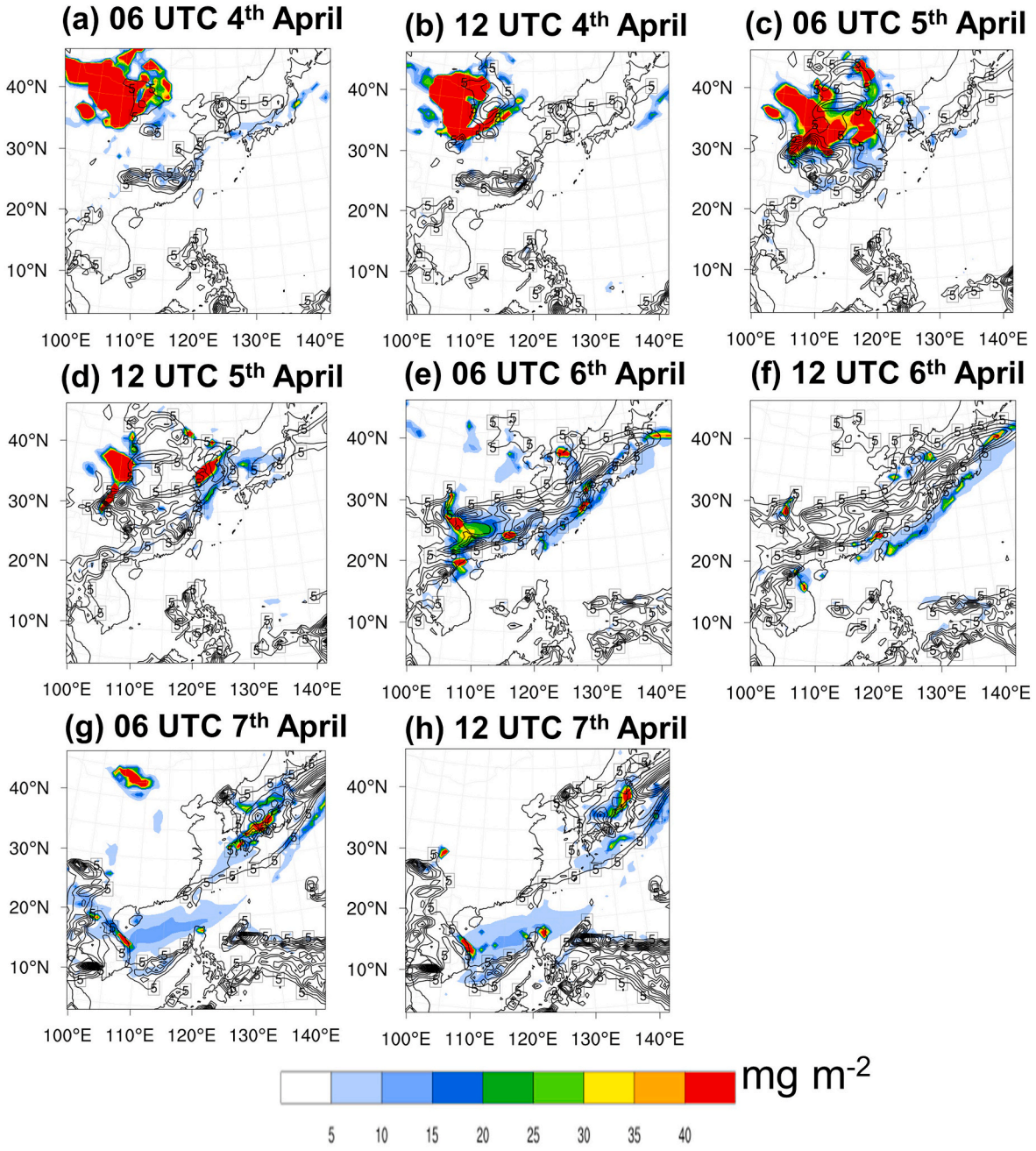

Fig. 10. Spatial distribution of the precipitation (dark contour from 5 to 50 mm by 5 mm) and total deposition flux for (a,c,e,g) 06 UTC and (b,d,f,h) 12 UTC during (a–b) 4th, (c–d) 5th, (e–f) 6th and (g–h) 7th April 2018.

prevailing wind under HPPC circulated clockwise and local winds were northeasterly in northern Taiwan (Fig. 7a). From the DUST_Modified_3 treatment, it is apparent the model successfully simulated suspension and uplifting of the dust plume to the 500 hPa pressure level, followed by transport to northern Taiwan, which is located at more than 2000 km from the source region (Fig. 7a and b). Our simulation suggested a higher altitude of dust aerosol transport of 500 hPa over the source region compared to the height mentioned by Chen et al. (2017) and Hu et al. (2019). In order for the dust particles to transport over the distance from northwest China to transboundary downwind locations, the dust particles need to remain at a high altitude of the free atmosphere for an extended period of time (Tsai et al., 2008).

Initially, the dust plume was lifted up over the Gobi Desert at 00 UTC 4th April 2018. The surface synoptic map suggested an intense surface High (H in Fig. 7a) of 1034 hPa to the east and a weak surface Low (L in Fig. 7a) of 1003 hPa on the south edge of the dust source region. The strong pressure gradient as shown in Fig. 7a caused the strong wind speed over the Gobi Desert, and eventually triggered the dust emission over the area.

PM_{10} vertical profiles (Fig. 8) show the dust event extending from the source region in northern China towards the coastal area of eastern China, along a transect drawn as a purple line in Fig. 1a. Fig. 8a and b illustrate the ascending motion of dust particles from the surface layer towards the upper level at 500 hPa over a 4-h period (22 UTC 3rd – 02 UTC 4th April 2018), and transported along the maximum altitude of 326 K potential temperature isentropic. In the southern Gobi Desert, the dust plume reached its maximum height along the 500 hPa (~5 km) trough on 02 UTC 4th April as shown by the synoptic weather map in Fig. 8b. The dust plume reached Taiwan region 55 h later and descended on northern Taiwan at 11 UTC 6th April (Fig. 7d).

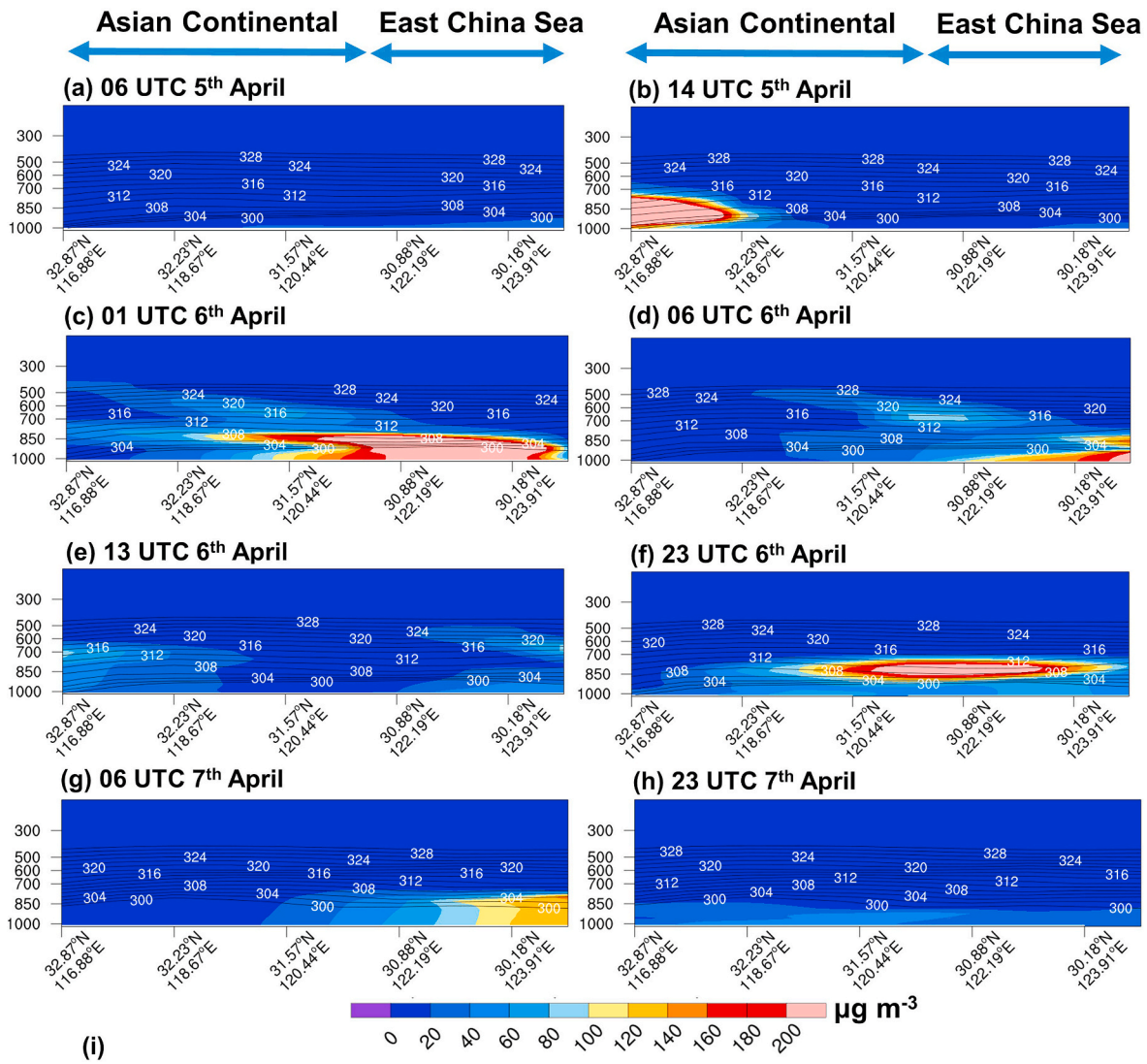

Fig. 11. Spatial distribution of potential temperature (dark contour from 300 to 330 K by 2 K) and vertical cross section of PM_{10} concentrations (along the red line transect shown in Fig. 1(a)) at (a) 06, (b) 14 UTC 5th April 2018, (c) 01, (d) 06, (e) 13 UTC (f) 23 UTC 6th April 2018, (g) 06 UTC and (h) 23 UTC 7th April 2018; (i) is the corresponding time series of PM_{10} maximum mass concentrations. (For interpretation of the references to color in this figure legend, the reader is referred to the Web version of this article.)

Table 5
Variations of PM_{10} along the transect of the red line in Fig. 2a.

Period (refer to Fig. 9)	Change (μg m^{-3})	Changes (%)	Rate (μg m^{-3} h^{-1})
a → b	373.10	1123.80	46.63
b → c	−96.50	−23.75	−8.77
c → d	−136.70	−44.12	−22.78
c → e	−209.90	−67.75	−17.49
e → f	176.40	176.57	17.64
f → g	−114.50	−41.44	−16.35
f → h	−206.90	−74.88	−8.62

In fact, the model simulated two dust plumes arriving to northern Taiwan 20 h apart (Fig. 4f and g). Fig. 7d shows the first dust plume reaching northern Taiwan at 11 UTC 6th April 2018, followed by the second plume at 07 UTC 7th April 2018 (Fig. 7g). The occurrence of the second plume can be explained by the synoptic weather map in Fig. 7a, which shows a low-pressure system over northeastern China on 5th April 2018, a full day after the first plume was emitted from the source region. This cyclonic system uplifted the dust aerosol from the Gobi Desert surface in northern China to the 700 hPa and 500 hPa pressure levels (Fig. 9b and c), and spread further to the east. The dust particles were suspended at that altitude for more than 10 h, then diffused downward by a strong northwesterly wind to the ocean surface, and eventually to the ground level at northern Taiwan on 07 UTC 7th April 2018.

As shown in Fig. 7e, the second dust plume did not reach the surface layer of Shanghai. The PM_{10} concentrations were generally greater than 60 μg m^{-3} across Shanghai and the nearby region as shown in the black dashed-circle. However, the concentrations of PM_{10} were greater than 200 μg m^{-3} at the 800 hPa layer along the trough system (Fig. 7f). High PM_{10} concentrations were carried by the northwesterly wind towards the southeastern region, and eventually deposited over the East China Sea (Fig. 7g). As a result, only a very small amount of PM_{10} managed to reach northern Taiwan.

5. Dust transport and deposition in East Asia

As we had already modified the dust generation component of the model in various ways, we had to assume that the continued underestimation might be due to an overestimated loss in the model; hence, this section analyzes the LRT path of the dust aerosols and details the dust deposition process over the domains. In general, our simulation suggested that the total deposition of the dust aerosol over the Asian Continent was larger than over the ocean, contributing 73.4% and 26.6% to total deposition, respectively. Our result was similar to the modeling results from Zhang et al. (2018), who used Weather Research and Forecasting with Chemistry (WRF-Chem) model, where the deposition flux across the Asia-Pacific region was 75.6% over land and 24.4% over the ocean. Fig. 10a–c shows the total deposition as greater than

Table 6
Comparison of WRF and observed precipitation in Shanghai.

	Daily total precipitation (mm day^{-1})		
	5th April 2018	6th April 2018	7th April 2018
Observation	16.76	0.00	0.00
WRF	20.78	31.38	0.00
Bias (%)	24.00	100.00	0.00

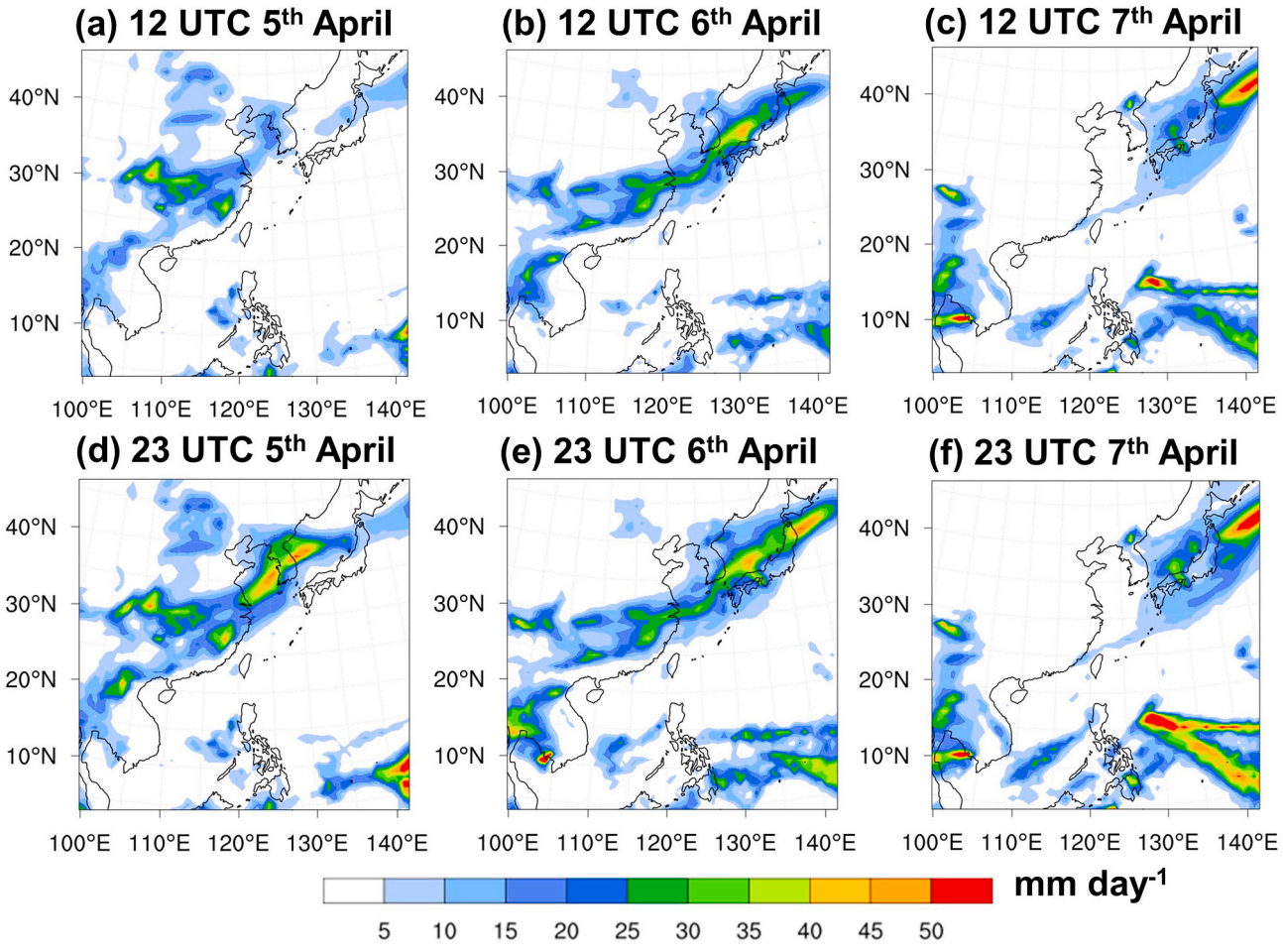

Fig. 12. Daily total precipitation over East Asia in 12 UTC (a, b, c) and 23 UTC (d, e, f), during (a) 5th, (b) 6th and (c) 7th April 2018, respectively.

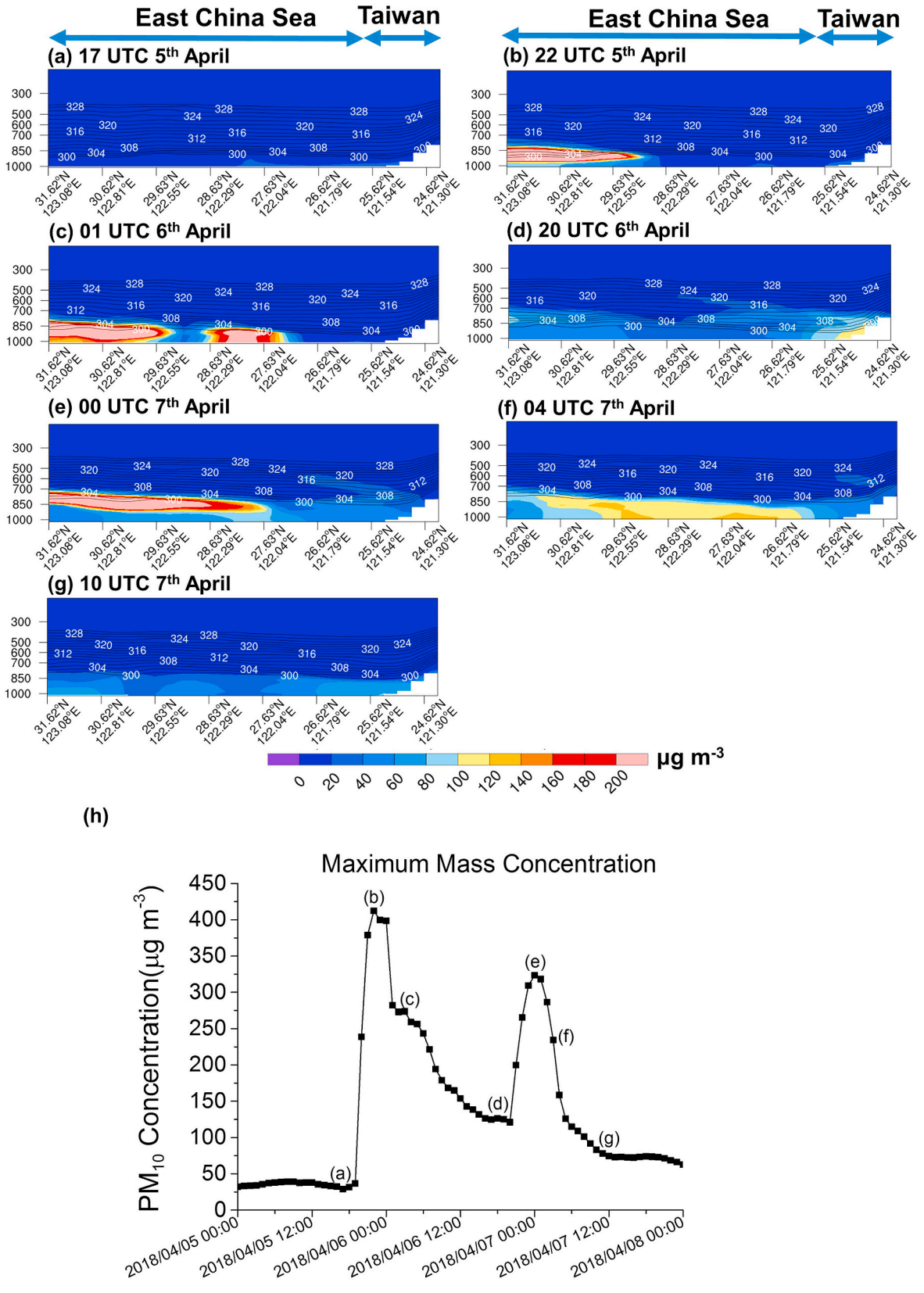

Fig. 13. Spatial distribution of potential temperature (dark contour from 300 to 330 K by 2 K) and vertical cross section of PM_{10} concentrations (along the dashed-red line shown in Fig. 1(a)) at (a) 17, (b) 22 UTC 5th April 2018, (c) 01, (d) 20 UTC 6th April 2018, (e) 00, (f) 04, (g) 10 UTC 7th April 2018 and (h) is the corresponding time series of PM_{10} maximum mass concentrations. (For interpretation of the references to color in this figure legend, the reader is referred to the Web version of this article.)

Table 7
Variations of PM_{10} along the transect of the yellow line in Fig. 2a.

Period (refer to Fig. 11)	Change (μg m^{-3})	Changes (%)	Rate (μm^{-3} h^{-1})
a → b	383.40	1322.06	76.68
b → c	−130.20	−31.57	−43.4
b → d	−161.20	−70.65	−7.32
d → e	202.50	167.35	50.62
e → f	−164.90	−50.97	−41.22
e → g	−288.30	−89.11	−8.47

40.0 mg m^{-2} over northern China. Further downwind the dust deposition flux was more widely distributed over southern China and the ocean (Fig. 10d–h), where the corresponding spatial pattern was coherent with the precipitation contour. The dust aerosol concentration spatial distribution exhibited a similar pattern to the deposition flux, consistent with the findings by Tan et al. (2017). In other word, regions with higher precipitation amount have higher dust depositions and PM_{10} concentrations especially over the downwind area.

The dust aerosols were then transported towards the East China Sea, passing the coastal area of East China (red line in Fig. 1a) on 5th–7th April 2018. Modeled vertical cross-sections of this transect are shown in Fig. 11, indicating that initially there was no significant amount of suspended dust at 06 UTC 5th April 2018 (Fig. 11a). At 14 UTC 5th April 2018, a dust plume entered the transect area (Fig. 11b), with the maximum mass concentration increased by 1123.80% (a → b in Table 5). The dust plume moved over the east coast of continental Asia at the 500 hPa level (~5 km) in the subsequent 10 h (Fig. 11c). During this time (14 UTC 5th April to 01 UTC 6th April), the maximum PM_{10} mass concentration was gradually decreased by 23.75% (b → c in Table 5), along the altitude of 316 K potential temperature isentropic. The model then demonstrated a dramatic reduction in PM_{10} concentration between 01 and 13 UTC 6th April 2018 (Fig. 11c–e) by 67.75% of the maximum mass concentration (c → e in Table 5). Several studies have mentioned that underestimation of the dust emission is the main factor leading to the modeled PM_{10} underpredicted results (Chuang et al., 2008b, 2019; Skyllakou et al., 2014); however, our analysis indicates the underestimation could be due to PM_{10} deposition in the marine boundary layer.

Excessive dust deposition onto the ocean surface could be caused by wet deposition, specifically by cloud washout and rainfall interception of suspended dust particles (Li et al., 2011; Tan et al., 2017; Zhang et al., 2017). Fig. 10 shows the dust outflow region including coastal eastern China, Japan, Korea and Taiwan experiencing significant dust deposition flux. This situation is closely associated with the spatial distribution of the total precipitation at the surface (Li et al., 2011). Fig. 12 shows the daily total precipitation over the study domain from the WRF model. On 5th April 2018, the modeled high precipitation >25.0 mm was found covering Japan, Korea, East China Sea and Sea of Japan (Fig. 12a and d). The pattern became more obvious on 6th April 2018, when a significant rainfall belt stretched from northeast Japan towards eastern China in a southwest direction (Fig. 12b and e). This may be the main reason for the modeled PM_{10} underestimation in northern Taiwan, suggesting a large portion of PM_{10} deposited to the ocean surface before it could reach northern Taiwan. As a result, the modeled dust plume entered northern Taiwan with a maximum total concentration of 222.8 μg m^{-3} at 11 UTC 6th April 2018 (Figs. 4b and 7d). Table 6 presents the comparison between the modeled and observed (from the US National Climate Data Center, NCDC) daily total precipitation in Shanghai during the dust event, with the modeled rainfall overestimating the observed rainfall on 5th and 6th April 2018. As a result, we believe that the over-prediction of modeled rainfall is one of the reasons causing the excessive dust deposition near Shanghai and underestimation of PM_{10} in both Shanghai and northern Taiwan. At 23 UTC 6th April 2018, a second dust plume entered the red transect at an altitude below 700 hPa (Fig. 11f). PM_{10} concentrations then were significantly reduced by 74.88% as illustrated in Fig. 11f and h. Different from the first plume, the concentration decrease of the second dust plume was not related to wet deposition, since total daily rainfall on 7th April 2018 was insignificant (Fig. 12c and f)). Thus, we looked into other meteorological processes such as wind speed that could affect dry deposition of the dust particles.

Fig. 13 presents the vertical cross section of PM_{10} concentrations passing over the East China Sea on its way to northern Taiwan, along the transect represented by the yellow line in Fig. 2a. The purpose of this analysis was to depict the LRT of PM_{10} concentrations over the ocean surface. PM_{10} was dramatically reduced by 70.65% (b → d in Table 7) between 22 UTC 5th and 20 UTC 6th April 2018 (Figs. 13b and 14d). By 01 UTC 6th April 2018, the first dust plume had been split into two (Fig. 13b), due to washout/rainout associated with heavy precipitation as shown in Fig. 12b. Then, the second dust plume from the source region reappeared at 00 UTC 7th April, which indicates the second dust plume also originated from the Asian continent and reached the East China Sea (Fig. 13e). However, the dust aerosol concentration in the second plume was significantly reduced by 89.11% (e → g in Table 7) during 01 UTC 6th– 00 UTC 7th April 2018 (Fig. 13e and g). As shown in

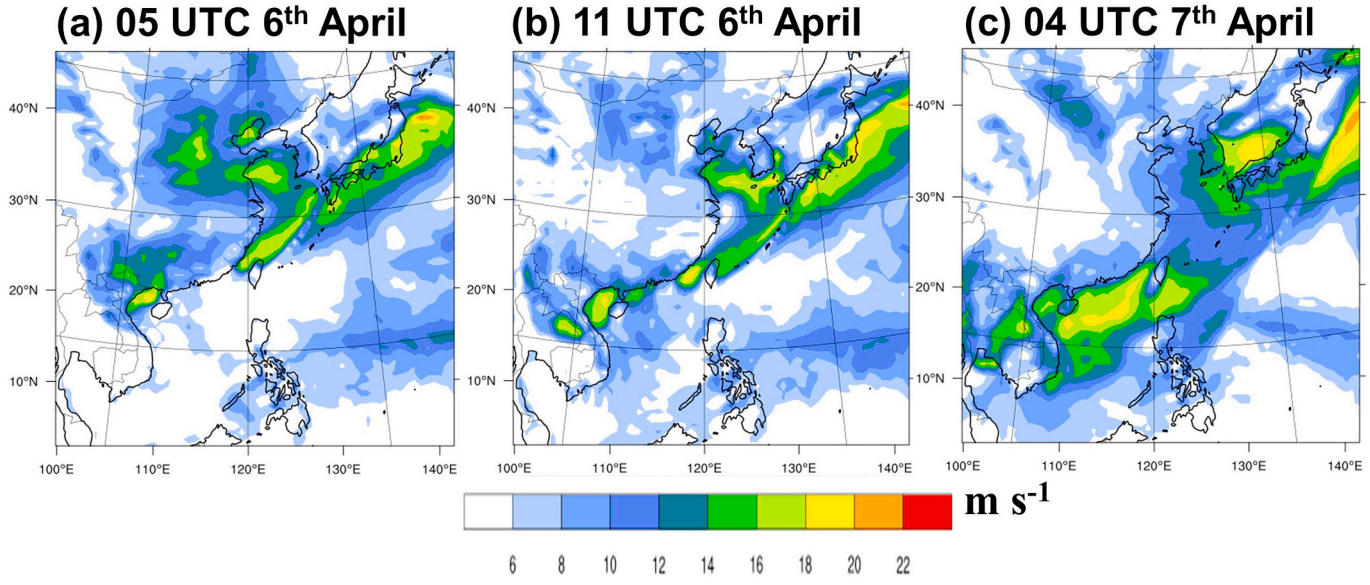

Fig. 14. Wind speed over East Asia at (a) 05 UTC, (b) 11 UTC 6th April 2018 and (c) 04 UTC 7th April 2018.

Fig. 13f, the PM_{10} deposition flux was intensive over the ocean surface during that time.

Recent studies (Li et al., 2012; Tan et al., 2017) have suggested that wet deposition plays an important role in reducing the dust particle concentrations over the dust outflow region, which contrasts with the second dust plume simulated in our study. Unlike wet deposition, which is dependent on precipitation, dry deposition is solely dependent on gravitational sedimentation. By this mechanism, large particles are more easily removed during LRT, leaving a greater contribution from smaller particles during transport to the downwind region. In our simulation, as there was no significant rainfall during transport of the second plume over the ocean (Fig. 12c), we suggested that the sudden PM_{10} reduction (Fig. 13f) was due to dry deposition (Guo et al., 2019).

Moreover, there was a positive relationship between the dust aerosol pattern and the intensity of the 10-m wind speed (Guo et al., 2019). Fig. 14 presents the wind speed spatial distribution during transport of the dust plumes over the ocean surface. An intense wind speed >16.0 m s^{-1} was observed over Japan, Korea and East China Sea on 6th April at the time of the first plume. Over the Taiwan Strait, such high wind speed is expected to transport the PM_{10} to northern Taiwan. However, due to the intense rainfall belt shown in Fig. 12b, e, wet deposition occurred over the area. On the other hand, lower wind speeds <12.0 m s^{-1} were observed over the East China Sea and Taiwan Strait at 04 UTC 7th April 2018 (black circle in Fig. 14c) at the time of the second plume, which exposed the dust particles to higher dry deposition fluxes in the model. As a result, we propose that dry deposition may be more significant when the average wind speed drops below some threshold (e.g. < 12.0 m s^{-1}). As relative to the high wind speed, the low wind speed condition could hardly carry the dust particle along the transport pathway; hence, the dust particles could easily deposit to the marine surface layer by gravitational sedimentation.

In previous studies involving CMAQ simulations with the dust treatment have suggested that dust emission and transport occurs when the friction velocity is less than the threshold friction velocity (Dong et al., 2016; Foroutan et al., 2017). To note, the windblown dust treatment (Foroutan et al., 2017) recalculated the friction velocity. In our study, the simulated dust emissions were sufficient and instead dry deposition due to the low wind speed distributed the dust particles over the marine boundary layer. Moreover, the dust treatment removes dust aerosols in the atmosphere at any rainfall over 0.254 mm or 0.01 in, and any rainfall amount below that value mentioned is considered a trace amount (Lebo and Seinfield, 2011; Foroutan et al., 2017). Consequently, the rainfall belt simply wiped out the entire plume of transported dust outflow from the Asian continent. As a result, we suggest the deposition mechanisms for the CMAQ dust treatment should be revised for use over the marine boundary layer, to reduce the uncertainty in the dust outflow region.

6. Conclusions

This study modified the new windblown dust emission treatment by Foroutan et al. (2017) and analyzed the long-range transport of East Asian Dust to Taiwan during 4th–9th April 2018. Compared to previous high PM_{10} episodes, this event was closely related to high wind speeds (9–13 m s^{-1}) over northern Taiwan immediately preceding the dust plume, and a prevailing south-westerly wind in northern China. By incorporating the new dust treatment without modification (default), the CMAQ simulation of PM_{10} performed only slightly better than without the module. By adjusting the soil moisture correction factor and dust composition profile in the dust treatment (Dust_Modified_3), the model significantly improved on the NMB to −23.43% from −78.51% in the default scheme. Our evaluation results were in agreement with several modeling studies including Dong et al. (2016) and Foroutan et al. (2017). Moreover, it is vital for the dust particles to uplift to the 500 hPa pressure level over northern China to have sufficient time in the atmosphere for transport to Taiwan region (Tsai et al., 2008). This modeling study suggested that large amounts of dust particles deposited onto the East China Sea and Taiwan Strait before reaching northern Taiwan, and is the primary reason for the modeled PM_{10} underestimation. Wet deposition occurred due to a significant modeled rainfall belt stretching from northeast Japan to eastern China in a southwest direction, intercepting the dust plume during transport to the south. Furthermore, deposition of the second dust plume occurred due to low wind speeds slowing its transport and leading to increased dry deposition of the dust particles. The weak wind speed was likely not enough to buoy the dust aerosol passing over the marine area. Hence, dust aerosol concentrations were reduced by 70.65% and 89.11%, mostly due to the modeled rainfall and weak wind speed, respectively. It is suggested that the CMAQ simulations can be improved by incorporating the new revised dust emission treatment from this study for projecting the long-range transport of dust particles over East Asia. Friction velocity and marine boundary layer precipitation were the major factors disrupting the dust module in this study, and should be carefully taken into account when implementing the dust treatment for transport over the ocean. Moreover, the indirect and direct effects between dust particles and cloud cover might inhibit or enhance the rainfall pattern, which could impact the dust simulation (Huang et al., 2014). It is recommended to implement the dust-cloud-precipitation interactions to the model in quantifying the aerosol feedback for the future studies.

CRediT authorship contribution statement

Steven Soon-Kai Kong: Conceptualization, Methodology, Formal analysis, Writing – original draft, Writing – review & editing. **Joshua S. Fu:** Conceptualization, Methodology, Supervision. **Xinyi Dong:** Data curation. **Ming-Tung Chuang:** Conceptualization, Methodology, Supervision. **Maggie Chel Gee Ooi:** Formal analysis. **Wei-Syun Huang:** Data curation. **Stephen M. Griffith:** Formal analysis. **Shantanu Kumar Pani:** Formal analysis. **Neng-Huei Lin:** Visualization, Supervision, Funding acquisition.

Declaration of competing interest

The authors declare that they have no known competing financial interests or personal relationships that could have appeared to influence the work reported in this paper.

Acknowledgments

We acknowledged the Ministry of Science and Technology of Taiwan, under the Project No. of MOST 108-2811-M-008-591 and Taiwan Environmental Protection Administration under the Project No. of EPA 1091G015 for supporting the research. We also gratefully acknowledged the US National Centers for Environmental Prediction (NCEP) for providing the Global Forecast System (GFS) data.

Appendix A. Supplementary data

Supplementary data to this article can be found online at https://doi.org/10.1016/j.atmosenv.2021.118441.

References

Appel, K.W., Pouliot, G.A., Simon, H., Sarwar, G., Pye, H.O.T., Napelenok, S.L., Akhtar, F., Roselle, S.J., 2013. Evaluation of dust and trace metal estimates from the Community Multiscale Air Quality (CMAQ) model version 5.0. Geosci. Model Dev. (GMD) 6 (4), 883–899. https://doi.org/10.5194/gmd-6-883-2013.

Bian, H., Tie, X., Cao, J., Ying, Z., Han, S., Xue, Y., 2011. Analysis of a severe dust storm event over China: application of the WRF-dust model. Aerosol Air Qual. Res. 11 (4), 419–428. https://doi.org/10.4209/aaqr.2011.04.0053.

Chang, J.C., Hanna, S.R., 2004. Air quality model performance evaluation. Meteorol. Atmos. Phys. 87, 167–196. https://doi.org/10.1007/s00703-003-0070-7.

Chen, S., Huang, J., Kang, L., Wang, H., Ma, X., He, Y., Yuan, T., Yang, B., Huang, Z., Zhang, G., 2017. Emission, transport and radiative effects of mineral dust from

Taklimakan and Gobi Deserts: comparison of measurements and model results. Atmos. Chem. Phys. 17 (3), 1–43. https://doi.org/10.5194/acp-17-2401-2017.
Chuang, M.T., Chiang, P.C., Chan, C.C., Wang, C.F., Chang, Y.Y., Lee, C.T., 2008a. The effects of synoptical weather pattern and complex terrain on the formation of aerosol events in the greater Taipei area. Sci. Total Environ. 399, 128–146. https://doi.org/10.1016/j. scitotenv.2008.01.051.
Chuang, M.T., Fu, J.S., Jiang, C.J., Chan, C.C., Ni, P.C., Lee, C.T., 2008b. Simulation of long-range transport aerosols from asian continent to taiwan by a southward asian high-pressure system. Sci. Total Environ. 406, 168–179. https://doi.org/10.1016/j.scitotenv.2008.07.003.
Chuang, M.T., Ooi, M.C., Lin, N.H., Fu, J.S., Te, Lee C., Wang, H., Yen, M.C., Kong, S.S.K., Huang, W.S., 2019. Study the impact of three Asian industrial regions on $PM_{2.5}$ in Taiwan and the process analysis during transport. Atmos. Chem. Phys. 20, 14947–14967. https://doi.org/10.5194/acp-20-14947-2020.
Crooks, J.L., Cascio, W.E., Percy, M.S., Reyes, J., Neas, L.M., Hilborn, E.D., 2016. The association between dust storms and daily non-accidental mortality in the United States, 1993–2005. Environ. Health Perspect. 124 (11), 1735–1743. https://doi.org/10.1289/EHP216.
Darmenova, K., Sokolik, I.N., Shao, Y., Marticorena, B., Bergametti, G., 2009. Development of a physically based dust emission module within the Weather Research and Forecasting (WRF) model : assessment of dust emission parameterizations and input parameters for source regions in Central and East Asia. J. Geophys. Res. Atmos. 114, 1–28. https://doi.org/10.1029/2008JD011236.
Dong, X., Fu, J.S., Huang, K., Tong, D., Zhuang, G., 2016. Model development of dust emission and heterogeneous chemistry within the Community Multiscale Air Quality modeling system and its application over East Asia. Atmos. Chem. Phys. 16, 8157–8180. https://doi.org/10.5194/acp-16-8157-2016.
Dong, X., Fu, J.S., Huang, K., Zhu, Q., Tipton, M., 2019. Regional climate effects of biomass burning and dust in East Asia: evidence from modeling and observation. Geophys. Res. Lett. 46 https://doi.org/10.1029/2019GL083894.
Eguchi, K., Uno, I., Yumimoto, K., Takemura, T., Shimizu, A., Sugimoto, N., Liu, Z., 2009. Trans-pacific dust transport : integrated analysis of NASA/CALIPSO and a global aerosol transport model. Atmos. Chem. Phys. 9, 3137–3145. https://doi.org/10.5194/acp-9-3137-2009.
Emery, C., Tai, E., Yarwood, G., 2001. Enhanced Meteorological Modeling and Performance Evaluation for Two texas Episodes. Report to the Texas Natural Resources Conservation Commission. ENVIRON, International Corp, Novato, CA.
Foroutan, H., Young, J., Napelenok, S., Ran, L., Appel, K., Gilliam, R., Pleim, J., 2017. Development and evaluation of a physics-based windblown dust emission scheme implemented in the CMAQ modeling system. J. Adv. Model. Earth Syst. 9, 585–608. https://doi:10.1002/2016MS000823.
Fu, X., Wang, S.X., Cheng, Z., Xing, J., Zhao, B., Wang, J.D., Hao, J.M., 2014. Source, transport and impacts of a heavy dust event in the Yangtze River Delta, China, in 2011. Atmos. Chem. Phys. 14, 1239–1254. https://doi.org/10.5194/acp-14-1239-2014.
Gelaro, R., McCarty, W., Suárez, M.J., Todling, R., Molod, A., Takacs, L., et al., 2017. The modern-Era Retrospective analysis for Research and applications, version 2 (MERRA-2). J. Clim. 30 (14), 5419–5454. https://doi.org/10.1175/JCLI-D-16-0758.1.
Ghim, Y.S., Kim, J.Y., Chang, Y.S., 2017. Concentration variations in particulate matter in Seoul associated with Asian dust and smog episodes. Aerosol Air Qual. Res. 17, 3128–3140. https://doi.org/10.4209/aaqr.2016.09.0414.
Guenther, A.B., Jiang, X., Heald, C.L., Sakulyanontvittaya, T., Duhl, T., Emmons, L.K., Wang, X., 2012. The Model of Emissions of Gases and Aerosols from Nature version 2.1 (MEGAN2.1): an extended and updated framework for modeling biogenic emissions. Geosci. Model Dev. (GMD) 5, 1471–1492. https://doi.org/10.5194/gmd-5-1471-2012.
Guo, J., Xu, H., Liu, L., Chen, D., Peng, Y., Yim, S.H.-L., Yang, Y.J., Li, J., Zhao, J., Zhai, P., 2019. The trend reversal of dust aerosol over East Asia and the North Pacific Ocean attributed to large-scale meteorology, deposition, and soil moisture. J. Geophys. Res. Atmos. 124 (10), 450–10,466 https://doi.org/10.1029/2019JD030654.
Han, X., Ge, C., Tao, J., Zhang, M., Zhang, R., 2012. Air quality modeling for of a strong dust event in East Asia in march 2010. Aerosol Air Qual. Res. 12, 615–628. https://doi.org/10.4209/aaqr.2011.11.0191.
Hu, Z., Huang, J., Zhao, C., Bi, J., Jin, Q., Qian, Y., Leung, L.R., Feng, T., Chen, S., Ma, J., 2019. Modeling the contributions of Northern Hemisphere dust sources to dust outflow from East Asia. Atmos. Environ. 202, 234–243. https://doi.org/10.1016/j.atmosenv.2019.01.022.
Huang, K., Zhuang, G.S., Li, J.A., Wang, Q.Z., Sun, Y.L., Lin, Y.F., Fu, J.S., 2010. Mixing of Asian dust with pollution aerosol and the transformation of aerosol components during the dust storm over China in spring 2007. J. Geophys. Res. Atmos. 115, D00K13. https://doi:10.1029/2009JD013145.
Huang, J., Wang, T., Wang, W., Li, Z., Yan, H., 2014. Climate effects of dust aerosols over East Asian arid and semiarid regions. J. Geophys. Res. Atmos. 119 (19), 11,398–11,416. https://doi.org/10.1002/2014JD021796.
Jiang, N., Dong, Z., Xu, Y.Q., Yu, F., Yin, S.S., Zhang, R.Q., Tang, X.Y., 2018. Characterization of PM10 and PM2.5 source profiles of fugitive dust in Zhengzhou, China. Aerosol Air Qual. Res. 19, 314–319. https://doi.org/10.4209/aaqr.2017.04.0132.
Jing, Y., Zhang, P., Chen, L., Xu, N., 2017. Integrated analysis of dust transport and budget in a severe Asian Dust Event. Aerosol Air Qual. Res. 17, 2390–2400. https://doi.org/10.4209/aaqr.2017.05.0170.
Kok, J.F., Parteli, E.J., Michaels, T.I., Karam, D.B., 2012. The physics of wind-blown sand and dust. Rep. Prog. Phys. 75 (10), 106901.
Lebo, Z.J., Seinfeld, J.H., 2011. Theoretical basis for convective invigoration due to increased aerosol concentration. Atmos. Chem. Phys. 11, 5407–5429. https://doi:10.5194/acp-11-5407-2011.
Li, J., Han, Z., Zhang, R., Asia, E., 2011. Model study of atmospheric particulates during dust storm period in March 2010 over East Asia. Atmos. Environ. 45 (24), 3954–3964. https://doi.org/10.1016/j.atmosenv.2011.04.068.
Li, M., Zhang, Q., Kurokawa, J., Woo, J., He, K., Lu, Z., Ohara, T., 2017. MIX : a mosaic Asian anthropogenic emission inventory under the international collaboration framework of the MICS-Asia and HTAP. Atmos. Chem. Phys. 17, 935–963. https://doi.org/10.5194/acp-17-935-2017.
Miller, R.L., Cakmur, R.V., Perlwitz, J., Geogdzhayev, I.V., Ginoux, P., Koch, D., Kohfeld, K.E., Prigent, C., Ruedy, R., Schmidt, G.A., Tegen, I., 2006. Mineral dust aerosols in the NASA Goddard Institute for Space Sciences ModelE atmospheric general circulation model. J. Geophys. Res. Atmos. 111 (6), 1–19. https://doi.org/10.1029/2005JD005796.
Park, S., Choe, A., Park, M., 2012. A simulation of Asian dust events in March 2010 by using the ADAM2 model. Theor. Appl. Climatol. 107 (3), 491–503. https://doi.org/10.1007/s00704-011-0494-9.
Shao, Y., Yang, Y., 2005. A scheme for drag partition over rough surfaces. Atmos. Environ. 39 (38), 7351–7361. https://doi.org/10.1016/j.atmosenv.2005.09.014.
Shao, Y., Ishizuka, M., Mikami, M., Leys, J.F., 2011. Parameterization of size-resolved dust emission and validation with measurements. J. Geophys. Res. 116, D08203. https://doi:10.1029/2010JD014527.
Skyllakou, K., Murphy, B.N., Megaritis, A.G., Fountoukis, C., Pandis, S.N., 2014. Contributions of local and regional sources to fine PM in the megacity of Paris. Atmos. Chem. Phys. 14, 2343–2352. https://doi.org/10.5194/acp-14-2343-2014.
Tan, S., Li, J., Che, H., Chen, B., Wang, H., 2017. Transport of East Asian dust storms to the marginal seas of China and the southern North Paci fi c in spring 2010. Atmos. Environ. 148, 316–328. https://doi.org/10.1016/j.atmosenv.2016.10.054.
Tian, P., Zhang, L., Ma, J., Tang, K., Xu, L., Wang, Y., Cao, X., Liang, Y.J., Jiang, J.H., Yung, Y.L., Zhang, R., 2018. Radiative absorption enhancement of dust mixed with anthropogenic pollution over East Asia. Atmos. Chem. Phys. 18, 7815–7825. https://doi.org/10.5194/acp-18-7815-2018.
Tsai, F., Chen, G.T., Liu, T., Lin, W., Tu, J., 2008. Characterizing the transport pathways of Asian dust. J. Geophys. Res. Atmos. 113, 1–15. https://doi.org/10.1029/2007JD009674.
Tsai, F., Fang, Y., Huang, S., 2013. Case study of Asian dust event on March 19-25, 2010 and its impact on the marginal Sea of China. J. Mar. Sci. Technol. 21 (3), 353–360. https://doi.org/10.6119/JMST-013-0326-1.
Uno, I., Osada, K., Yumimoto, K., Wang, Z., Itahashi, S., Pan, X., Hara, Y., Yamamoto, S., Nishizawa, T., 2017. Importance of long-range nitrate transport based on long-term observation and modeling of dust and pollutants over East Asia. Aerosol Air Qual. Res. 17, 3052–3064. https://doi.org/10.4209/aaqr.2016.11.0494.
Vukovich, J., Pierce, T., 2002. The implementation of BEIS3 within the SMOKE modeling framework. In: Proceedings of the 510 11th International Emissions Inventory Conference, Atlanta, Georgia, April 15–18, 2002.
Wang, S.H., Tsay, S.C., Lin, N.H., Hsu, N.C., Bell, S.W., Li, C., Ji, Q., Jeong, M.J., Hansell, R.A., Welton, E.J., Holben, B.N., Sheu, G.R., Chu, Y.C., Chang, S.C., Liu, J.J., Chiang, W.L., 2011. First detailed observations of long-range transported dust over the northern South China Sea. Atmos. Environ. 45 (27), 4804–4808. https://doi.org/10.1016/j.atmosenv.2011.04.077.
Wang, K., Zhang, Y., Nenes, A., Fountoukis, C., 2012a. Implementation of dust emission and chemistry into the Community Multiscale Air Quality modeling system and initial application to an Asian dust storm episode. Atmos. Chem. Phys. 12 (21), 10209–10237. https://doi.org/10.5194/acp-12-10209-2012.
Wang, S.H., Hsu, N.C., Tsay, S.C., Lin, N.H., Sayer, A.M., Huang, S.J., Lau, W.K.M., 2012b. Can Asian dust trigger phytoplankton blooms in the oligotrophic northern South China Sea? Geophys. Res. Lett. 39 (5) https://doi.org/10.1029/2011GL050415.
Wang, K., Zhang, Y., Nenes, A., Fountoukis, C., 2012c. Implementation of dust emission and chemistry into the Community Multiscale Air Quality modeling system and initial application to an Asian dust storm episode. Atmos. Chem. Phys. 12, 10209–10237. https://doi:10.5194/acp-12-10209-2012, 2012a.
Xu, P., Zhang, J., Ji, D., Liu, Z., Tang, G., Hu, B., Jiang, C., Wang, Y., 2017. Evaluating the effects of springtime dust storms over Beijing and the associated characteristics of sub-micron aerosol. Aerosol Air Qual. Res. 17, 680–692. https://doi.org/10.4209/aaqr.2016.05.0195.
Zhao, C., Liu, X., Leung, L.R., Hagos, S., 2011. Radiative impact of mineral dust on monsoon precipitation variability over West Africa. Atmos. Chem. Phys. 11 (5), 1879–1893. https://doi.org/10.5194/acp-11-1879-2011.
Zheng, B., Tong, D., Li, M., Liu, F., Hong, C., Geng, G., Li, H., Peng, L., Qi, J., Yan, L., Zhang, Y., Zhao, H., Zheng, Y., He, K., Zhang, Q., 2018. Trends in China' s anthropogenic emissions since 2010 as the consequence of clean air actions. Atmos. Chem. Phys. 18, 14095–14111. https://doi.org/10.5194/acp-18-14095-2018.